Journal of Environmental Chemical Engineering 11 (2023) 109783

Contents lists available at ScienceDirect

Journal of Environmental Chemical Engineering

journal homepage: www.elsevier.com/locate/jece

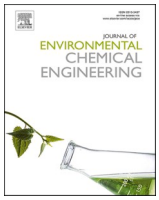

Optimizing hydrothermal dechlorination of PVC in a SS-316 reactor: From chemistry knowledge to material considerations

Mohammad Salimi *, Thomas Helmer Pedersen, Lasse Rosendahl

AAU Energy, Aalborg University, Pontoppidanstræde 111, 9220 Aalborg Ø, Denmark

ARTICLE INFO

Editor: Javier Marugan

Keywords:
PVC
Dechlorination
Plastic chemical recycling
Waste treatment
Corrosion
DOE

ABSTRACT

PVC remains one of the most challenging wastes for environmental activists and industrial recyclers because its decomposition products cause severe corrosion to equipment and our planet. The current study was designed to systematically investigate PVC dechlorination using the well-known Response Surface Methodology (RSM) to mature the process chemistry and assess the corrosion rate in the common SS-316 alloy. Undercover non-catalytic experiments, Cl removal, reactor wall corrosion rate, and H/C molar ratio of the products made the most argument to comprehend the chemistry and find the optimum operating condition. Based on data collected from different analytic techniques, like FESEM, SEM-EDX, TG, FT-IR, CHN, and AAS, it was found that water drove Cl removal through a combination of S_N2 and Elimination pathways where the in-situ production of hydrochloric acid at high Severity Factor (SF) resulted in a desirably high dechlorination rate of 89.42%. However, significant metal leakage into the aqueous phase, e.g., 278.01 mg of Fe, in the Aqueous Phase (AP) necessitated the valorization of different approaches, including multistage dechlorination and application of various hetero and homogeneous catalysts, dealing with chloride and metal salts inside the reaction chamber. Among the solutions applied, the dual-stage and Ni-assisted dechlorination showed promising performances receptively with a corrosion rate as low as 0.034 g and the highest Cl removal efficiency of 96.18%.

1. Introduction

To avoid squandering the money, energy, and time invested in plastics manufacturing and to mitigate the negative effects of its waste on the environment, human beings would have no choice but to care restrictively about the fate of these polymeric materials [1]. Among the well-known 6 R rule options, recycling may be the most promising, at least from a technological standpoint, because returning polymeric waste material to industrial plants can effectively prevent energy leakage. Although the need for plastic recycling is undeniable, selecting the appropriate recycling technology turned out to be critical [2].

Polyvinyl chloride (PVC), with its unique properties such as high stability in different environments and the ability to exhibit a wide range of plastic-elastic properties when mixed with plasticizers and additives, has a high demand and accounts for 12% of total plastic production [3]. At the molecular level, PVC has a linear head-to-tail structure formed via free radical addition polymerization with typical number-average molecular masses of 50000–120000 g mol^{-1}. However, the release of chlorine-containing organics upon its degradation has caused PVC to be a threat to both living entities and facilities[4].

To deal with PVC wastes, the most mature technologies to date are mechanochemical recycling, pyrolysis, and low-temperature catalytic dechlorination in the presence of metal oxides; however, almost all these techniques suffer from a couple of common drawbacks, including the formation of chlorinated solids, the release of HCl in the reaction medium, and formation of chlorinated liquid products which frequently require further fining [5,6]. Many research groups have concentrated their efforts on chlorine removal from recycling chambers to address and overcome these challenges [3,7–9]. Using the adsorption capacity of HCl scavengers, many attempted to entrap the chlorides released during the recycling process [10]. This path, however, has been abandoned due to its high complexity and, in most cases, very low efficiency in practice. In terms of dechlorination, PVC in the (thermo)chemical process follows one of the post-hydrotreatment or pre-hydrodechlorination pathways.

The most significant disadvantage of the former approach is the negative impact of an acidic environment on the conversion rate, as PVC degradation at elevated temperatures commonly results in 10–20% coke formation [3]. Previous research demonstrated that PVC is the only

* Corresponding author.
E-mail address: msali@energy.aau.dk (M. Salimi).

https://doi.org/10.1016/j.jece.2023.109783
Received 9 December 2022; Received in revised form 16 February 2023; Accepted 23 March 2023
Available online 25 March 2023

halogenated polymer that undergoes pronounced charring reactions rather than liquefaction reactions due to acidic conditions [11]. Some discovered a solution by neutralizing the reaction medium with alkali agents [12]. However, no significant differences in oil and solid yields were obtained, with the main difference measured in gas and Aqueous Phase (AP) yields. These ongoing challenges have finally given newcomers, particularly those equipped with a pre-dechlorination step, the opportunity to play a key role in the technology [13].

HTL processing of PVC at low temperatures and pressure has demonstrated great promise in recovering solid residues with much lower chlorine content, making PVC further conversion in incineration or other thermochemical plants more efficient [14–16]. However, reactor corrosion remains a critical barrier in the process of industrialization. Is-situ formation of hot concentrated hydrochloric acid, because of Cl migration to the AP, exacerbates reactor wall corrosion mainly through promoting the flaking of the reactor's dense oxide layer [17]. Even though all the contributions have been made up to date by utilization of high corrosion resistance alloy materials of 316 L[18] and Inconel 625[19], the only outcome has been limited to a significant increase in the overall cost.

To overcome the low reaction rate in water, which is said to be 150 times slower than dechlorination in PEG (a polar aprotic solvent that drives the reaction via the E2 mechanism), as well as to increase process safety, researchers have been considering the use of various homogeneous/heterogeneous catalysts [20,21]. NaOH, KOH, and $CaCO_3$ are some of the most common homogenous catalysts used to improve dechlorination efficiency and mitigate the corrosiveness of the reaction medium. Previous studies show that base catalysts can only marginally accelerate dechlorination because of their negative impact on polymer surface reactivity after a while of contact [22]. Regarding heterogeneous catalysts, the initial research focused on Pd-based catalysts supported primarily on well-known substrates such as Alumina[22]. Later, to replace the overpriced Pd particles, some catalysts based on Fe/Ni and copper were developed, with Ni being the most effective in the dechlorination of PVC liquid phase under mild conditions, such that after a significant reaction time (more than 5 h), all the chlorine is transferred into the aqueous product [23–25].

Even though severe corrosion of the reactor wall caused by the presence of HCl at high temperatures and pressure has called into question the validity of Hydrothermal Dechlorination (HTDC), experts continue to capitalize on the lack of any chlorinated organic compounds in the product stream as its main advantage [3]. Developing inexpensive corrosion-resistant materials might take a long time in material society; meanwhile, maturing process chemistry, with a great emphasis on corrosion mechanism, could be an important shortcut to a practical solution. Throughout the literature, one can hardly find a noticeable work paying well to the reactor wall corrosion from a process point of view, especially concerning PVC dechlorination. To this, the current study on HTDC of PVC stands out in the literature because it provides the scientific community with significant experimental and statistical information about how chlorine is removed from the polymeric chain. For the first time, we harnessed the Response Surface Methodology (RSM) not merely to optimize operating conditions for maximum dechlorination efficiency but to study the extent of corrosion that happens to the reactor wall through screening the role of Temperature (T), Reaction Time (RT), and water content in HTDC process. The current experimental strategy culminated in catalytic HTDC, in which various types of catalysts and approaches, ranging from homogeneous to heterogeneous catalysts, as well as multistage hydrothermal treatment, were used to go beyond the degree of dechlorination achieved under non-catalytic conditions. All these investigations were carried out undercover various analytic techniques, including Elemental analysis (CHN), Scanning Electron Microscopy (SEM), Fourier transform infrared (FTIR) spectroscopy, Atomic Absorption Spectroscopy (AAS), X-Ray diffraction (XRD), Electrochemical Chloride measurement, and Thermogravimetric analysis (TG).

2. Material and methods

2.1. Materials and reagents

The PVC used in this study was purchased from Sigma Aldrich as virgin polymer powder with no additives and was directly used in the HTDC process. The elemental and SEM-EDX analyses measured its Cl content as high as 61.19 wt%. Besides, concentrated Nitric Acid (70%), Polyvinyl Alcohol (PVA) (with a molecular weight of 89000–98000 and purity of >99%), and Silver Nitrate ($AgNO_3$) (0.1 M, with a purity of >99.9%) were all provided from Sigma Aldrich for Chloride measurement. Deionized water was the only liquid chemical used throughout the experimental outline as either a reaction medium or a solvent, and it was readily available.

In catalytic experiments, homogenous catalysts, like Potassium Carbonate (K_2CO_3, with a purity of ≥99.0%) and Nickel Nitrate Hexahydrate ($Ni(NO_3)_26\ H_2O$, with a purity of ≥ 98.5%), were used as they were collected from the vendor (Sigma-Aldrich). On the other hand, the heterogeneous catalyst, TiO_2 (anatase, with a purity of ≥99%), went through a couple of preparation steps, as will be described in *Section 2.3* .

2.2. HTDC process: from theory to practice

2.2.1. Control parameters and DOE/RSM procedure

The traditional, time-consuming, and inefficient One-Factor-At-A-Time method was to be replaced in this study with an optimized experimental design based on the DOE/RSM methodology using Stat-Design Ease's Expert application, version 10.0.4.0. The D-optimal criteria were used to investigate the interactions of the parameters influencing the dechlorination process. The tool minimizes the variance associated with the estimates of the specified model coefficients and provides optimal operating conditions with the fewest independent runs [26].

While the literature contains many valuable studies on the importance of Temperature (T) and Residence Time (RT) on the dechlorination of PVC, the effect of PVC concentration is yet to be understood [20, 27–29]. In practice, all these parameters went through three distinct levels where 20 randomized runs, designed by DOE software, were carried out to track the impact of each parameter and uncover any hidden interactions. Table 1 represents the main control factors, Temperature (factor A), Reaction Time (factor B), and Water/PVC ratio (factor C), and their corresponding discrete levels.

One advantage of using DOE is its ability to identify important terms in the model through analysis of variance (ANOVA). This feature also assists the user in determining the significance of a regression model based on the Fischer (F) test and probability (P) values. For a model to be significant, the highest possible F value must accompany a P value of less than 0.0500. Furthermore, P values greater than 0.1000 render the model terms insignificant. However, these two are not the only indicators of a significant model term, and it needs a reasonable R^2 (fairly close to One) to be reliable [26,30,31].

In the present work, the linear, 2FI, and quadratic models were fetched to the experimental data, including the Cl removal rate, Fe measurement, and Hydrogen/ carbon ratio (H/C molar ratio), and the best model was chosen so that P, F, and R^2 values agreed well. It should

Table 1
Main Control factors influencing γ-alumina co-precipitation process along to.

Process variables	Controlled Factor	Lower-Upper levels	Unit	Symbol
Temperature	A	200–250	°C	T
Reaction Time	B	15–60	Minute (min)	RT
Water/PVC ratio	C	2–15	ratio	W/PVC

be noted that the final regression equations only included significant actual factors.

2.2.2. HDTC experiments in practice

Table 2 shows the 20 randomized alternative runs, given by the DOE software, for non-catalytic HTDC of PVC (see Tables SM.4 and SM.5 in Supplementary Material File (SMF)). The experiments were carried out in two Swagelok micro-batch reactors made of SS-316 material, according to the randomized test orders that had been determined. To ensure the results' reproducibility, we repeated the experiments in duplicate, with the mean of the two independent experiments used as the main data. The full description of a real experiment is available in SMF under *section SM.1*.

Furthermore, because of the complex nature of the reaction network in the presence of subcritical water, a Severity Factor (SF) was thought to be critical in properly exploring the impact of operating parameters. HTDC of PVC is widely assumed to occur in an acidic environment, and such combined SF can be calculated using the following equation, which includes the pH term [32]:

$$\log SF = \log\left(RT.e^{\frac{(T-100)}{14.75}}\right) - pH \quad (1)$$

In this equation, RT is the reaction time in minutes, and T stands for the HTDC temperature in °C.[1]

2.3. Heterogenous catalyst preparation

The TiO_2 powder supplied by the vendor was first dried at 120 °C in an oven overnight to remove any moisture content trapped inside. Then the appropriate amount was weighed and calcined in the furnace at 400 °C for 4 h with a temperature ramp of 1 °C.min^{-1} under airflow.

2.4. Analytical techniques

2.4.1. Elemental analysis

C and H content of the solid samples were measured using a PerkinElmer CHN instrument (PerkinElmer 2400 Series II, USA) following the ASTM D5291–16 procedure [33]. Although the presence of Cl in the samples has made direct or differential oxygen measurements impossible, joint analysis of the samples with the SEM-EDX instrument enables practical oxygen measurement.

2.4.2. Surface chemistry and morphology

The nature of chemical functional groups found on the surface of solid residues was investigated using an FT-IR spectrometer (BRUKER, USA) in the 400–4000 cm^{-1} range. Furthermore, deploying an SEM device (SEM equipped with an Energy Dispersive Spectrometer (EDS) with a germanium detector, Oxford Instrument, England), the surface morphology and elemental distribution of the solid samples were investigated.

2.4.3. Chloride measurement

Because the reaction takes place in aqueous conditions and it is assumed that almost all of the removed Cl is transferred into the aqueous phase, titration with AgCl was thought to be the best option for measuring chloride removal. As a result, the chloride measurement was performed with the Carl Fischer instrument equipped with an AgCl 62 RG electrode, all manufactured by Xylem, UK. Appropriate amounts of HNO_3 (4.0 M) and PVA (0.5 M) were added to the analyte to free all the chloride ions before the mixture was titrated with $AgNO_3$ (0.1 M).

The following equation was used to calculate the Cl removal rate per unit mass of chlorine in the feed material:

$$Cl\% = \frac{(Cl_{product} - Cl_{pvc})}{Cl_{PVC}} \times 100 \quad (2)$$

In this equation, Cl% shows the chlorine removal rate from PVC, and Cl_i, i could either be PVC or Product, stands for the Chlorine content of the material under investigation.

The procedure for measuring chloride with the Xylem product is documented on the manufacturer's website [34].

2.4.4. Bulk characterization

Thermogravimetric (TG) analysis was carried out using TGA/SDTA851e microbalance instrument (Mettler Toledo, Switzerland) to track the thermal behavior of dechlorinated solid products. In practice, the temperature was ramped up to 1000 °C with a rate of 5 °C.min^{-1}, while the dry air passed through the sample at a flow rate of 50 ml.min^{-1}. The chamber gas was changed to O_2 for ash analysis when the temperature reached 600 °C. X-ray diffraction of corrosion products was recorded using a PW1840 diffractometer with monochromatized Cu/K radiation (Philips, Netherlands).

2.4.5. Corrosion measurement

Atomic Absorption Spectroscopy (AAS) was used to measure the Fe, Ni, Mo, and Cr contents in the aqueous products following procedures mentioned in [35]. The measured values accurately represent the intensity of corrosion to the reactor material (SS-316) that occurs during the HTDC process. Appropriate cathodic lamps with electromagnetic radiation wavelengths of 246.3, 303.8, 313.3, and 429.0 nm, respectively, corresponding to Fe, Ni, Mo, and Cr elements, were used for this measurement. A PinAAcle 900 F instrument (PerkinElmer 2400 Series II, USA) was used for the measurement.

3. Results and discussion

While almost all tables and figures with data from the ANOVA analyses are included in SMF (Figures SM.1–3 and Table SM.1–3), Table 3 summarizes how significant the fitted models are and how much each operating parameter affects chlorine removal from PVC as well as metal deterioration from SS-316 alloy. Such evaluation is founded upon the Cl removal rate, Fe-Ni-Cr concentration in AP, and H/C molar ratio in the solid products (Fig. 1-2). The following sections are devoted to interpreting the obtained results and optimizing optimum operating conditions for maximum Cl removal with the least corrosion impact.

3.1. Cl Removal

Given the P-value of less than 0.0001, adjusted R^2 of 0.9853,[2] and F value of 142.71, ANOVA analyses imply the significance of the quadratic model for Cl removal under the HTDC reaction condition. In line with the literature, Temperature and RT are the most important parameters affecting the process in the presence of water [13,14,28]. However, with a P value higher than the threshold (0.1000),[3] the W/PVC ratio counterintuitively turns out to be insignificant in the fitted Quadratic model, a critical finding that can challenge all the presumptions on the role of water in this process [36–38]. Furthermore, Fig. 1A clearly shows that T has a greater impact on the Cl removal rate than RT, implying a higher dechlorination efficiency (Red region) as a result of doing HTDC at moderate temperatures but longer RT.

3.2. H/C molar ratio

The information revealed by CHN analyses enlightens what happens to the elemental distribution in the chain structure when PVC is

[1] The values of the operating conditions were rounded up to be practically applicable on the experimental setup.

[2] To be significant, a model's "Adjusted R-Squared" should be maximized.

[3] The mentioned value is not shown in Table 2. Vide Tables SI.1–3 in SIF.

Table 2
Experimental outline of non-catalytic dechlorination of PVC and their corresponding results.

Exp.No	RXN Metadata	RXN Data				Fe (mg) in AP	Chloride Removal (%) in AP	H/C molar ratio
		SF	**W/PVC**	**T** (°C)	**RT** (min)			
1	HTDC_NC_02	2.02	13	210	24	1.23	1.26	1.24
2	HTDC_NC_05	2.82	7	210	24	2.5	1.53	1.72
3	HTDC_NC_11	4.15	10	225	37.5	28.21	12.63	1.28
4	HTDC_NC_12	4.05	5	225	37.5	43.54	9.31	1.45
5	HTDC_NC_06	3.29	7	210	51	3.46	2.38	1.68
6	HTDC_NC_17	3.99	13	210	51	3.45	2.17	1.61
7	HTDC_NC_14	4.15	10	225	37.5	27.41	13.21	1.34
8	HTDC_NC_16	4.15	15	225	37.5	15.89	9.01	1.56
9	HTDC_NC_04	4.15	10	225	37.5	20.20	8.64	1.43
10	HTDC_NC_09	4.15	10	225	37.5	51.15	11.76	1.25
11	HTDC_NC_08	3.35	10	225	15	9.74	5.47	1.52
12	HTDC_NC_15	4.45	10	225	60	185.14	54.97	1.55
13	HTDC_NC_18	4.15	10	225	37.5	17.48	9.78	1.75
14	HTDC_NC_19	4.15	10	225	37.5	26.28	11.71	1.46
15	HTDC_NC_13	2.41	10	200	37.5	1.28	0.92	1.33
16	HTDC_NC_03	4.15	13	240	51	244.93	79.10	1.46
17	HTDC_NC_10	4.90	7	240	51	222.11	78.20	1.55
18	HTDC_NC_07	4.72	7	240	24	229.53	82.87	1.46
19	HTDC_NC_20	4.70	13	240	24	191.83	69.75	1.46
20	HTDC_NC_01	4.99	10	250	37.5	278.01	89.42	1.42

Table 3
Fitting model and ANOVA analyses' results in terms of process variables.

Target parameter	Fitted Model/P-Value	Significant Terms/P-values	R^2	Equation
Cl Removal	Quadratic/ < 0.0001	A/< 0.0001, B< 0.0001, AB/0.0003, $A^2/< 0.0001$	0.9923	$\frac{1}{Cl\ removal(\%)} = +0.089 - 0.30A - 0.062B + 0.071AB + 0.17A^2$
Fe Corrosion	Quadratic/ < 0.0001	A/< 0.0001, B< 0.0001, AB/< 0.0001, $A^2/< 0.0001$, $B^2/ < 0.0440$	0.9907	$\frac{1}{\sqrt{Fe\ in\ AP(mg)}} = +6.41 - 7.65A - 1.64B + 1.70AB + 3.15A^2 - 0.43B^2$
H/C Molar Ratio	Linear/< 0.0001	A/< 0.0001, B< 0.0001	0.9400	$\sqrt{\frac{H}{C}molar\ ratio} = +1.21 - 0.064A - 0.026B$

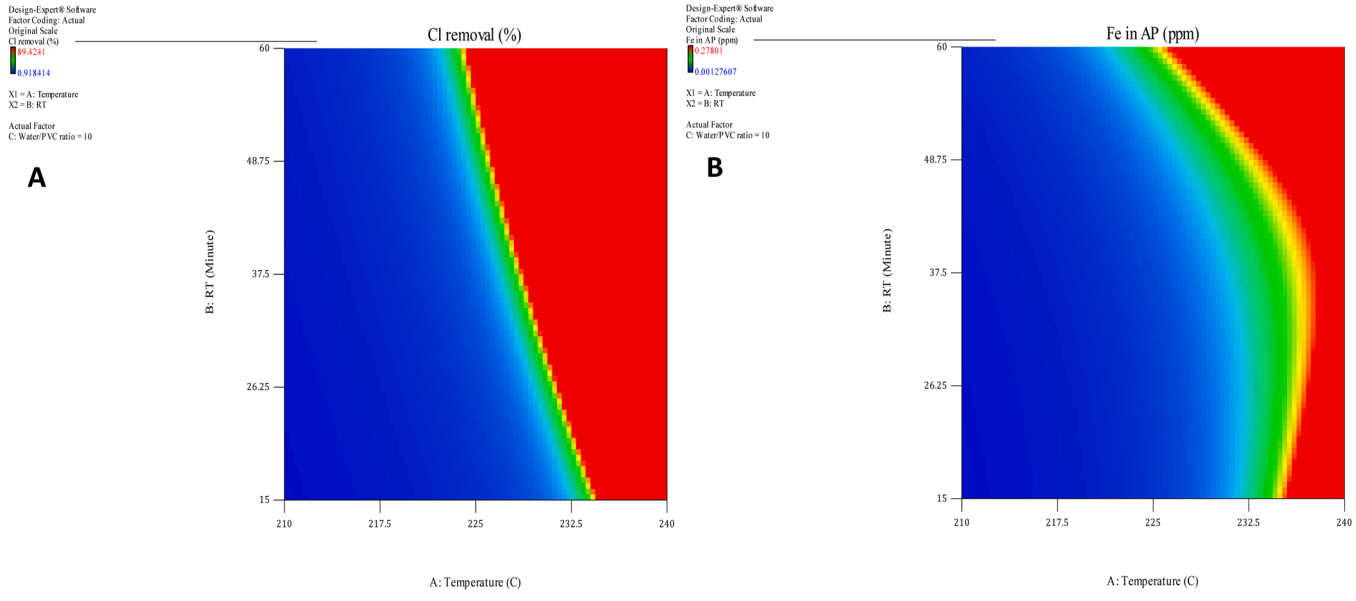

Fig. 1. Contour diagrams representing the impact of T vs. RT on; left) Cl removal from PVC and right) Fe detachment from reactor wall.

subjected to the HTDC treatment. The H/C molar ratio could also be of high importance since it is considered an indication of the unsaturation degree along the length of the carbonaceous backbone. Table SM.4 in SMF includes all figures regarding the CHN analyses.

Considering ANOVA analysis results (vide Table SM.3 and Figure SM.3 in SMF), the H/C molar ratio of the solid product changes linearly with the T and RT as the only significant factors. A P value of less than 0.0001, Adjusted R^2 of 0.9400, and Lack of Fit P-value of 0.2883 all made the Linear model best fit the experimental data in the case of H/C molar ratio.

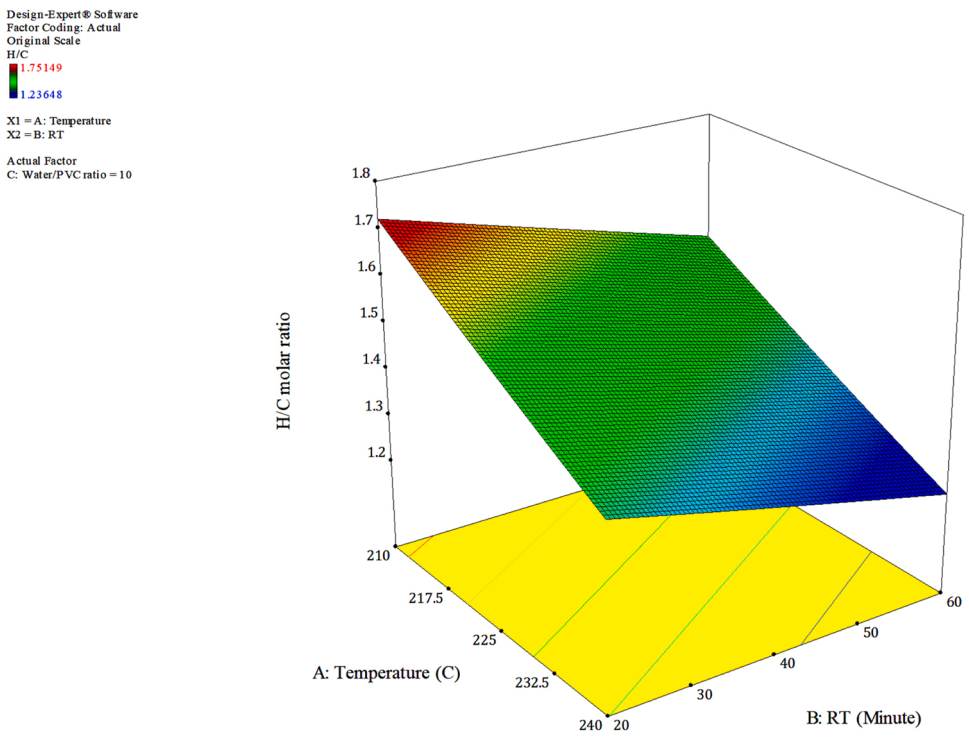

Fig. 2. 3D plot representing the impact of T vs. RT on the H/C molar ratio of solid products.

Throughout the literature, a high H/C molar ratio in hydrochars usually accompanies a high degree of Cl removal to uniquely feature the benefits of dechlorination in an aqueous environment [22]. Scientists reason the enhanced H/C atomic ratio for the nucleophilic substitution of Cl with OH groups where water plays the dual role of solvent and nucleophile at the same time. Water is considered a weak oxidative agent at room temperature, but as its temperature and pressure rise, it gains more oxidizing strength. Accordingly, water is expected to act as a moderate nucleophile in the HTDC environment driving dechlorination via the OH substitution (S_N2) mechanism proposed by a multitude of researchers [24,36,38]. However, in stark contrast, CHN results show a merely opposite trend in the solid samples of the HTDC test in the present work, which prompted us to reconsider the mechanism through which water takes part in the HTDC of PVC (see *Section 3.4*).

3.3. Impact of process severity

The most important findings from SEM-EDX analyses are summarized and illustrated in terms of the well-known van Krevelen diagrams in Fig. 3. This Figure unveils the significant impact of process severity on the dechlorination of PVC. A change in reaction severity from mild to the severe condition has significantly decreased H/C and Cl/C molar ratios. On the other hand, O/C and H/C molar ratios behave conversely, where an increase in severity has brought about a higher O/C molar ratio at the expense of a higher unsaturation degree.

From the surface chemistry viewpoint, Fig. 4 provides FT-IR spectra of two dechlorinated samples under two different reaction conditions, while patterns of all other samples can be found in Figure SM.4 in SMF. FT-IR spectra depicted in Fig. 4 look so similar that almost no difference could be observed in the shape and intensity of the peaks as the reaction severity changes; however, a closer examination reveals tiny differences at 1400–1700 cm^{-1}.

Having reviewed the literature, we attributed peaks in 600–800 cm^{-1} to the stretching mode of C-Cl bonds [39,40]. These peaks appear equally strong in spectra derived from HTDC_NC_01 and 13 samples, indicating a similar extent of dechlorination over the surface of PVC samples even under different HTDC operating conditions. This surface chemistry similarity may be related to the leveling effect of hot-compressed water, as will be discussed later by SEM-EDX results.

Aside from C-Cl bonds, the spectra in Fig. 4 nearly follow the pattern of PVC (vide Figure SM.4 in SMF) wherein C═C, C-O, and C-H bonds stretch/vibrate around their corresponding wavelengths (For more information on all notable peaks and their functional groups, refer to Table SM.6 in SMF) [41,42]. More intriguingly, there is a difference in peak intensity observed at wavelengths ranging from 1500 to 1600 cm^{-1}. To our knowledge, these peaks primarily belong to C═C aromatic vibrations, which do not exist in the spectrum of virgin PVC [43], proposing the formation of a new part in the solid products under severe operating conditions.

As compelling evidence, TG analyses provided outstanding information on how HTDC severity impacts the thermal robustness of virgin PVC (vide Figures SM.5–9 and Table SM.4).

The spider diagram in Fig. 5 shows that an increase in SF deliberately enhances the toughness of the solid product, so a higher amount of solid product withstands thermal treatment at a temperature higher than 350 °C. The fact that almost all organic chlorine is to be removed up to 300 °C can justify the lower weight loss in hydrochars remaining from dechlorination with high SF [38]. A high severity in HTDC of PVC, on the other hand, appears to result in a solid product almost concentrated in a highly stable network. The recent observation supports the above argument about forming an aromatic part in solid products under severe operating conditions.

3.4. HTDC mechanism

As a rule, it is assumed that PVC decomposes in two steps during hydrothermal treatment, beginning with dechlorination at $T < 280$ °C and ending with complete degradation of the dechlorinated polyene into low molecular-mass compounds at $T > 300$ °C [38]. Literature spots OH-nucleophilic substitution as the main chemical pathway for detaching Cl from PVC backbone at temperatures lower than 450 °C and high-water densities [10,22] since water can act as a powerful nucleophile under hot-compressed conditions. However, having put all information acquired from characterization analyses together, we propose a

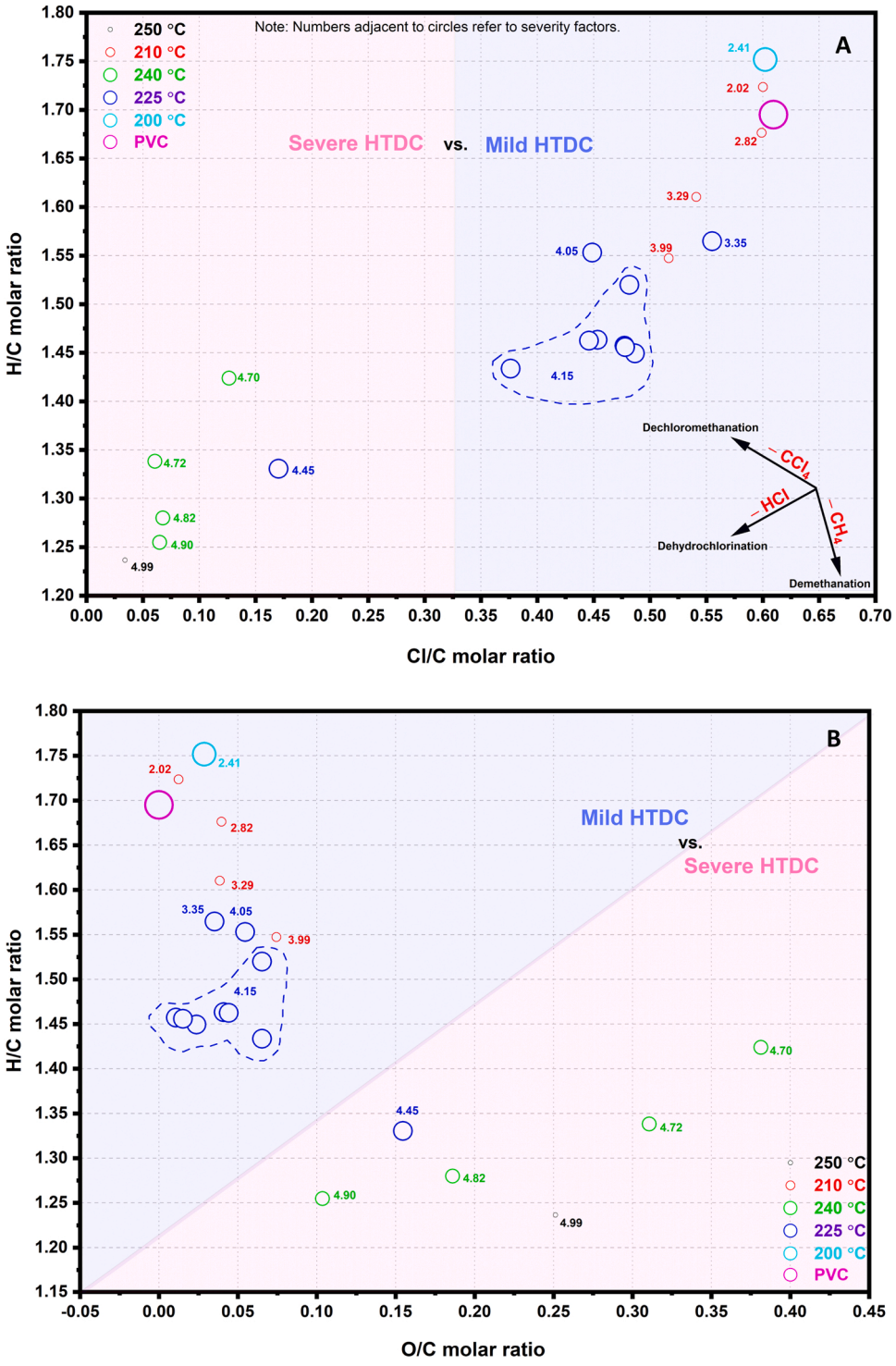

Fig. 3. van Krevelen diagrams of virgin PVC and solid products of HTDC process, A) Cl/C versus H/C and B) O/C versus H/C molar ratios. (Based on the data collected from CHN and SEM-EDX analyses).

dual functionality for water in the HTDC process as the severity of HTDC changes.

As shown in Fig. 3, the formation of a product with a slightly decreased Cl/C ratio (Fig. 3 A) and a considerable shift in H/C and O/C ratios (Fig. 3B) at temperatures as low as 200–210 °C indicates partial substitution of Chlorine atoms with OH groups. This could happen to a restriction of the S_N2 mechanism at low process severity (pathway I in Scheme1).

On the other hand, doing HTDC in severe mode leads to more efficient Cl removal through replacing Chlorine with OH nucleophiles (S_N2) followed by dehydration reaction (E1), where a slight increase in the SF from 4.70 to 4.72 when doing HTDC at 240 °C has led to a significant decrease in the O/C molar ratio (Fig. 3B).

Such Elimination could help the formation of polyenes through dehydration of the partially hydroxylated intermediates (Product D) when the reaction severity increases and medium acidity escalates. Others have also reported a similar observation where they found that HCl accelerates algae dehydration by decreasing the hydrogen content

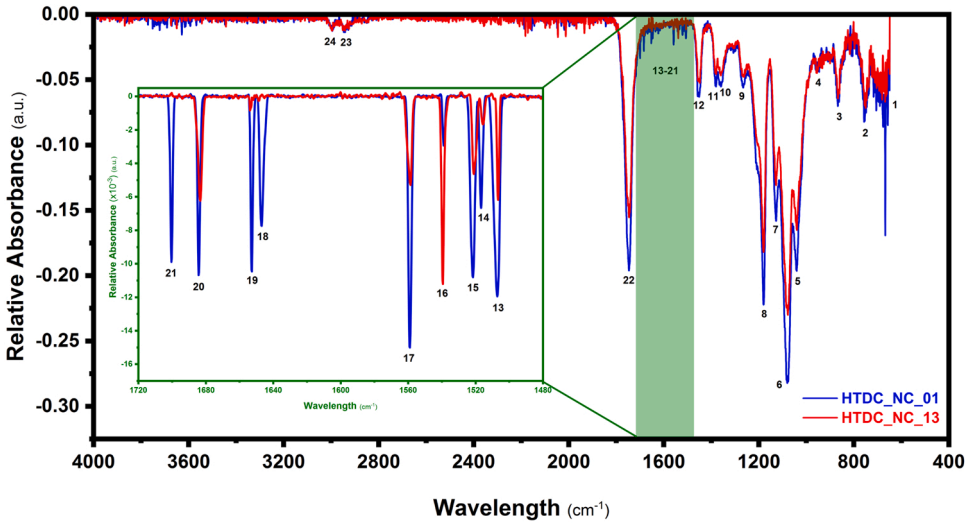

Fig. 4. FT-IR results for HTDC_NC_01 and HTDC_NC_13 solid residues.

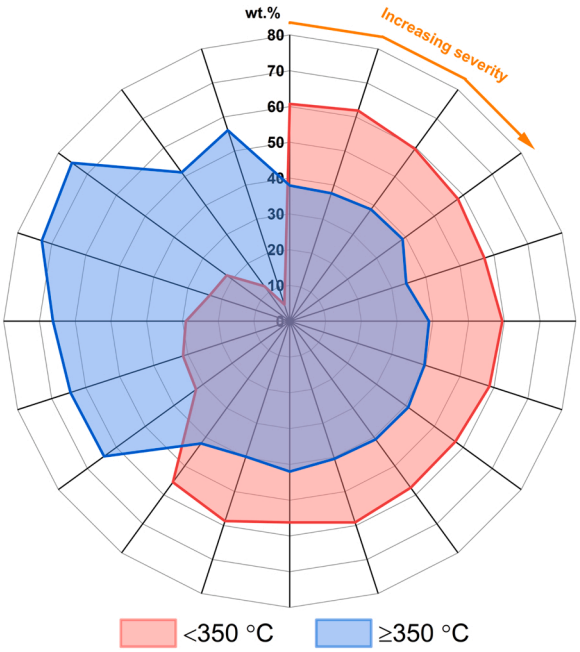

Fig. 5. Spider diagram showing the impact of the process severity on the thermal stability of the solid products.

in the final product [8]. It must be noted that performing HTDC of PVC at high temperatures, e.g., 250 °C for a considerable RT, could also drive the reaction through a fast E2 mechanism (Pathway III in Scheme 1); however, the extent of such reaction will be limited due to the presence of water.

3.5. Reactor wall corrosion

The presence of chlorine in the depolymerization/decomposition products causes severe corrosion to the downstream units and makes PVC one of the most difficult plastic wastes to deal with. It worsens when the chlorine leaks into an aqueous solution, forming hydrochloric acid. Thus, HTDC of PVC or any other Cl- containing organic moieties [24,25] inevitably involves corrosion, so the condition of the reactor wall must be monitored as precisely as the chlorine removal rate.

To investigate the extent of reactor corrosion in the HTDC process, we subjected all aqueous samples to AAS using the procedure described in Section 2.4.5. It must be noted that the reactor wall was rinsed several times after each experiment to collect any little chloride salts attached to the reactor wall. Iron, among the other metals, had the highest concentration in the AP of non-catalytic experiments. Hence, it served as the corrosion indicator when screening the corrosiveness of the process using DOE software. Other metals found in SS-316 alloy compositions, such as Ni and Cr, have also been thoroughly investigated. However, Molybdenum concentration in AP turned out to be under the AAS instrument's detection limit, i.e., less than 0.5 ppm.

Table 2 shows the experimental results for the measured milligrams of Fe in the AP (vide Table SM.2 and Figure SM.2 in SMF for ANOVA results). Throughout the ANOVA results, there is a good consistency and high accuracy among the experimental data where a P value of 0.0001, Adjusted R^2 of 0.9907, and a Lack of Fit of 0.4901 reinforce the fitted Quadratic Model. Statistics provided by RSM also argue that T and RT play key roles in the leakage of Fe molecules into the AP, and their interaction has a significant impact.

With respect to Fig. 1B, Fe leakage into AP is not almost visible at temperatures as low as 200 °C, whereas it increases significantly at 250 °C (278.0 mg). This is most likely attributed to the thermal degradation of PVC at this temperature region, as shown by TG results (Fig. 5). A similar trend could also be observed when tracking RT impact, where the Fe concentration in the liquid phase at all process temperatures increased with increasing time. Such impacts could be better understood by replacing SF for Temperature and RT, which involves pH as the third factor (see Section 2.2.2 for more information). Among metals in SS-316 alloy, Fig. 6A demonstrates that Iron had the highest contribution to the reactor wall corrosion products in the AP and, interestingly, cracked into the AP in a pattern like dechlorination. Therefore, the extent of Fe corrosion seems to be related to Cl removal, with the higher the dechlorination efficiency, the greater the Fe corrosion and consequently higher H_2 evolution via the following reaction (also see Fig. 6B):

$$Me_{(s)} + HCl_{(aq)} \rightarrow MeCl_{2_{(aq)}} + H_{2_{(g)}} \quad (3)$$

Where Me stands for metals, including Fe, Ni, and Cr.

In manufacturing high-alloy steel, experts formulate the final product to form an initial, thin, and protective oxide layer upon exposing highly corrosive conditions [44]. In the case of Chromium, previous studies show that it forms an initial oxide layer of Cr_2O_3 that will not react with HCl due to its high thermodynamic stability. However, HCl can crack into this layer and react with metals deep inside the reactor wall to form metal chlorides. Fig. 7 demonstrates SEM-EDX images and

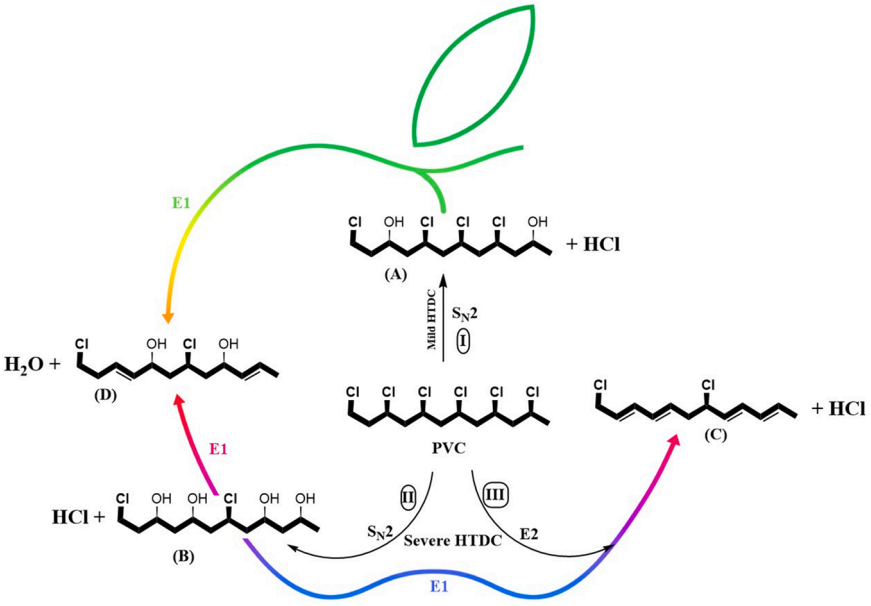

Scheme 1. Mechanism of S_N2 reaction and Ionic elimination for HTDC of PVC.

mappings corresponding to the reactor wall material (SS-316 alloy), displaying the distribution of Ni, Mo, Fe, Cr, Cl, and oxygen elements over the interior surface (Colorful elemental mapping in Fig. 7) and across the wall thickness of the reactor (Fig. 7D). In line with the published data [44], our findings spot Cr_2O_3 as the main compound covering the outer surface of SS-316 directly exposed to the HTDC environment. Fig. 7D well shows Iron depletion in the inner layers of the reactor due to higher corrosion rates upon direct exposure to HTDC medium.

This finding is supported by XRD results, where we analyzed the greenish corrosion product after scratching out of the reactor at the end of each reaction set. Fig. 8 depicts the corresponding diffractogram with phases symbolized schematically. Literature ascribes diffractions located at 23.1°, 26.1, 28.0°, and 30.9° to hematite (Fe_2O_3, JCPDS card No: 79–0007) [45], Cr_2O_3 (JCPDS no. 38–1479) [46], and magnetite (Fe_3O_4, JCPDS card 00–003–0863) [47] phases. The absence of metal chlorides in the XRD pattern could most likely be due to their hygroscopic nature, a feature that prevents metal chlorides from forming crystalline structures.

Likewise, metallic Ni existed in the corrosion product as the peaks at 2θ, 44.4°, and 51.6° suggest [48]. These two peaks could also have resulted from the presence of metallic Iron (JCPDS card No. 01–087–0721) [49] and Cr_2O_3; however, the existence of metallic Iron may be ruled out due to its tendency toward oxidation upon exposure to the highly oxidative hot-hydrochloric acid solution. One may assume that Nickel is prone to form oxides similarly; however, the peak at 51.6° reveals either the total or at least a proportion of Ni atoms remaining in the metallic phase. As a piece of compelling evidence, Schmid et al. [44] declined the formation of Nickel Chloride from metallic Ni existing in SS-316 alloy due to the positive Gibbs free energy for its chlorination.

Such findings help us readdress some previous observations where a few studies spotted Nickel chloride as the reason behind the green color of the AP collected from HTDC of PVC in stainless steel reactors [50]. The significantly higher contribution of Fe to the corrosion products and the high stability of metallic Ni in the reaction product implies that it might have been $FeCl_2$ salt that dominated the AP color as it dissolved in water in green color.

The above findings, combined with the knowledge available in the literature [44], drove us to propose the following corrosion mechanism for SS-316 alloy when exposed to the HTDC process, as shown schematically in Fig. 9.

In practice, it seems that hot-compressed HCl solution reacts with metals existing in the texture of SS-316 to produce corresponding metal chloride following Eq. 3. However, their reactivity upon exposure to such a corrosive medium in the presence of water made a difference in Fe, Ni, and Cr corrosion rates.

Previous thermodynamic calculations show that metal chloride formation is unlikely as the reaction escalates. In a study, Schmid et al. [44] argued that higher temperatures could lower the thermodynamic barrier for $CrCl_2$ reaction with water to form Cr_2O_3 via the following reaction:

$$3H_2O_{(l)} + CrCl_{2(s)} \rightarrow Cr_2O_{3(s)} + 2HCl_{(aq)} + H_{2(g)} \quad (4)$$

The same might happen to $FeCl_2$ via Eqs. 5 and 6, but one must consider that these reactions' highly positive Gibbs free energy restricts their extensive occurrence at T < 800 °C [44].

$$4H_2O_{(l)} + 3FeCl_{2(s)} \rightarrow Fe_3O_{4(s)} + 6HCl_{(aq)} + H_{2(g)} \quad (5)$$

$$3H_2O_{(l)} + 2FeCl_{2(s)} \rightarrow Fe_2O_{3(s)} + 4HCl_{(aq)} + H_{2(g)} \quad (6)$$

The protective Cr_2O_3 layer turned out to be porous, allowing HCl molecules to penetrate and reach metals deposited in the sublayer of SS-316 alloy. This has made Chromium atoms mainly remain on the surface of the reactor wall as oxidic Cr_2O_3 as the process severity escalates, while Fe leaked to the AP in the form of chlorides. Consequently, Fe shows a higher corrosion rate in AP despite having a lower position than Cr in the reactivity series of metals.

3.6. Mass transfer limitation in HTDC of PVC

Having reviewed the literature, one can find similar studies in which the authors argued the formation of polyene on the outer surface of solid products at higher temperatures and pressure that would impede dehydrochlorination because of the shielding effect [51]. The following discussion aims to clarify any potential impact of aromatization on mass transfer across PVC grains in terms of Cl removal. As a result, solid products were subjected to SEM-EDX analyses to investigate the radial distribution of elements along the intersection of PVC grains. The results of such studies are depicted in Fig. 10.

Fig. 10 depicts SEM-EDX results corresponding to HTDC_NC_04 and 13 samples, where radial distribution graphs clearly show the fluctuation in Cl concentration across grains on a micrometer scale. In line with previous studies [22,51], testaments provided here confirm a better

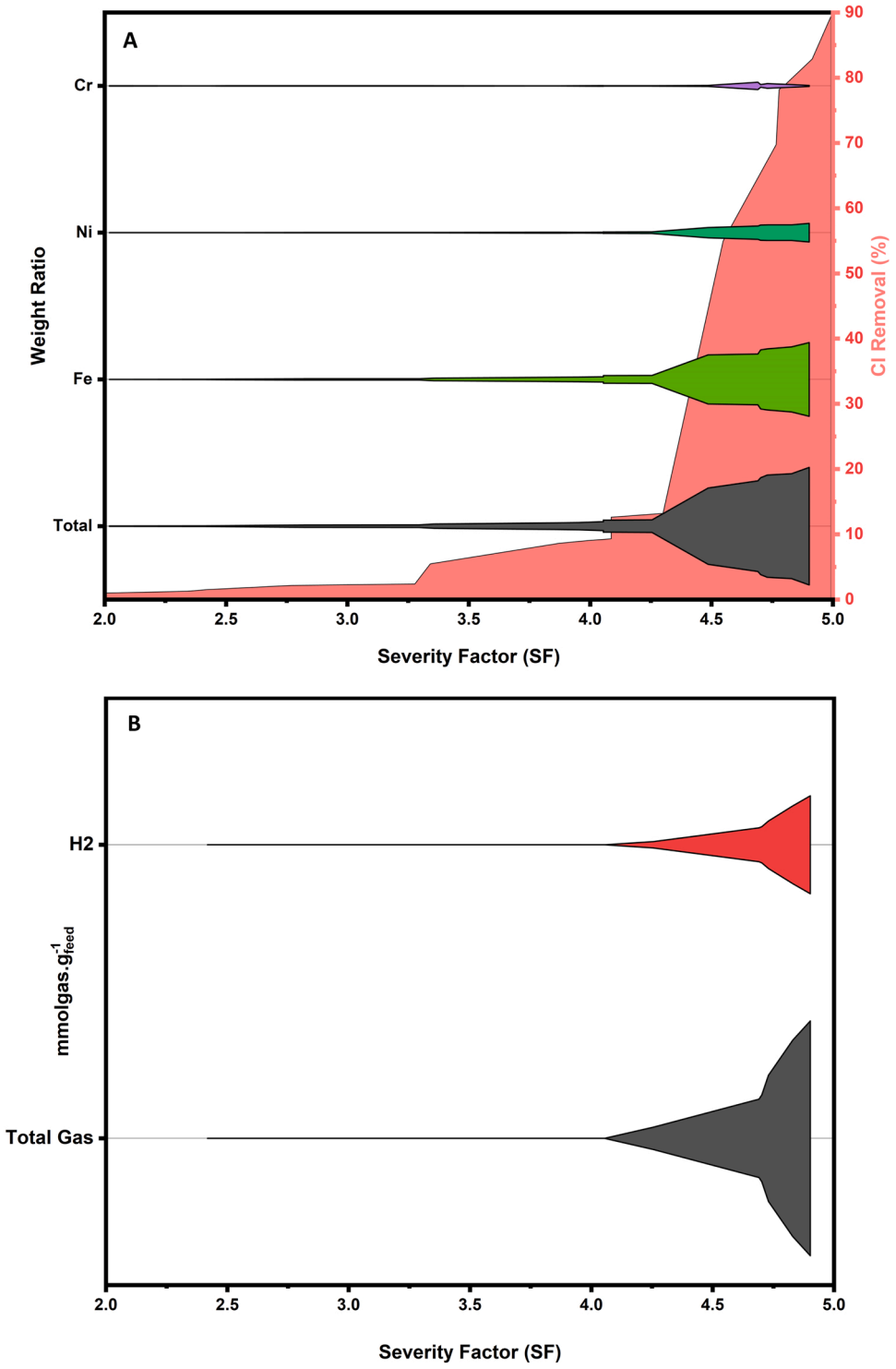

Fig. 6. The extent of SS-316 corrosion, Cl removal from PVC, and Gas production versus HTDC severity.

diffusion of water molecules through the so-called polyene shields as the reaction environment approaches the critical point. Such improved water molecule diffusion, combined with its increased oxidative/dehydrating activity, must have resulted in increased Cl removal, primarily via the substitution-elimination pathway, as shown in Scheme 1 (I and II pathways). Likewise, as the severity increases, HCl molecules have a greater opportunity to accelerate the E1 elimination of remaining Cl molecules in the PVC backbone and wear away the reactor wall via the corrosion mechanism depicted in Fig. 9.

3.7. CCD optimization

So far in this study, it has become apparent that implementing high T and RT would result in the greatest dechlorination while potentially promoting reactor wall corrosion. This observation prompted us to impose a few constraints to make the optimum solutions provided by the CCD tool more realistic (see Table SM.7 in SMF).

Table 4 depicts the predicted optimal operating conditions for achieving the highest possible Cl removal while keeping reactor corrosion to a minimum. This table also includes the calculated and actual

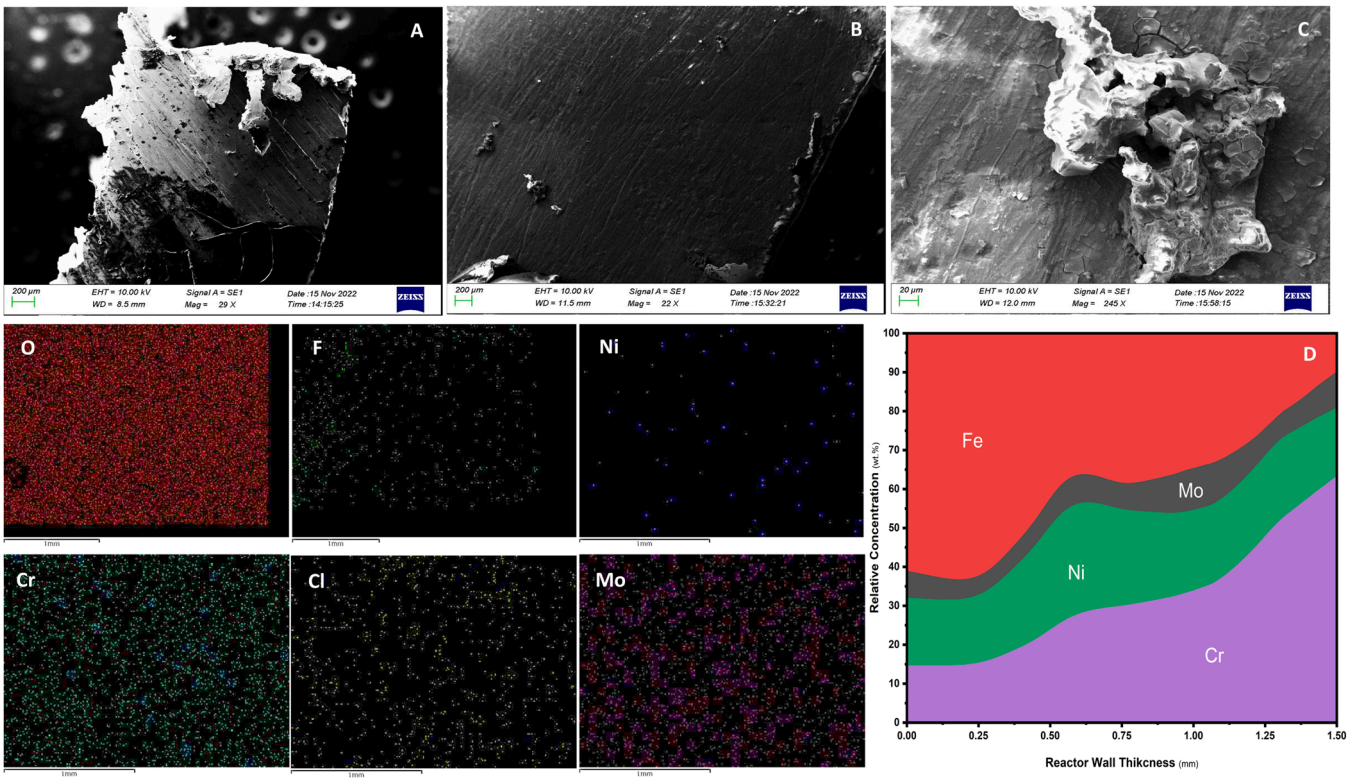

Fig. 7. Corrosion on the Reactor wall. A, B, and C) SEM images, and D) Radial distribution of SS-316 elements over reactor wall intersection. In part D, zero thickness represents the outer layer of the reactor, and 1.5 mm stands for the layers exposed to the HTDC process inside the reactor.

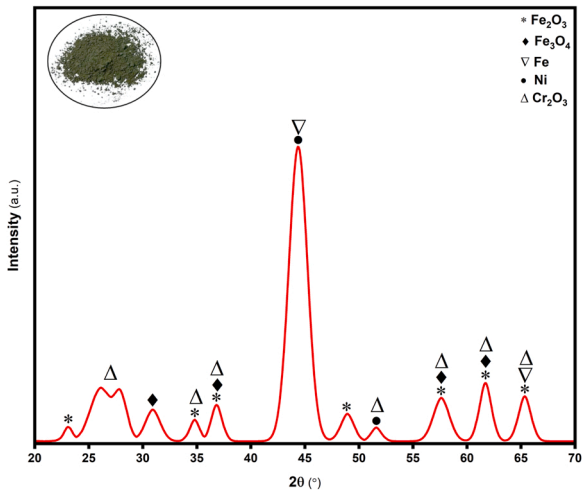

Fig. 8. XRD pattern of corrosion product derived from non-catalytic HTDC of PVC.

results obtained from CCD optimization and running the experiment under optimal operating conditions. The high consistency of actual results with the RSM predicted ones, with an error of less than 5.0%, validates the model fitted for all Cl removal, Fe in AP, and H/C molar ratio responses.

The Danish government's most recent data ensure that the Cl concentration in the Danish plastic waste stream does not exceed 27,500 ppm [10,52] (for detailed information, vide *section SM.2* in SMF). Following the 1000 ppm limitation many European countries have put in action for Cl contamination in the final RDFs, the HTDC process must be capable of removing 96.7% of the chlorine in the feedstock if it wants to pay a contribution to the technology in the future. While the non-catalytic tests did not report any Cl removal rates greater than 90%, we approached the goal using a different hypothesis from catalytic HTDC to doing the same process in dual stages mode. Ways that follow are intended to improve the rate of Cl removal and, at the same time, minimize reactor corrosion.

3.8. Catalytic HTDC of PVC

While some homogeneous catalysts, such as Ni^{2+} and K_2CO_3, have been extensively studied in the literature for PVC dechlorination[9,27], TiO_2 was barely exerted in the HTDC process. TiO_2 has shown its potential in the joint recycling of polyvinyl chloride in subcritical water with coal ash and coal mass where it was used in traces [53].

The most important results obtained from catalytic HTDC of PVC are represented in Table 5 and Figs. 11–13. In addition, Table SM.8 in SMF includes all experimental data for the catalytic part.

3.8.1. Elemental analysis

Starting with the Cl removal rate, the exerted catalysts showed various behavior when exposed to the HTDC environment. While Ni nearly doubled dechlorination efficiency from 35.49 ± 1.06–78.74 ± 3.12%, others acted as negative catalysts, decreasing chlorine removal efficiency compared to the optimal non-catalytic test (HTDC_NC_OPT).

In the case of the HCl evolution route, some authors claimed that the in-situ generated HCl acts as a self-catalyzer for PVC dechlorination. In contrast, others believed that the generation of HCl restricts the activation of catalysts and plays an important role in inhibiting the dechlorination rate [22,54]. The observed inactivity of the K_2CO_3 and TiO_2 catalysts in accelerating the Cl removal rate may be due to such pH damping impact by these materials.

Such distinctive impacts could also be observed from the H/C, O/C, and Cl/C molar ratios. TiO_2 and K_2CO_3 resulted in a similar H/C molar ratio but a higher Cl/C molar ratio than optimum non-catalytic

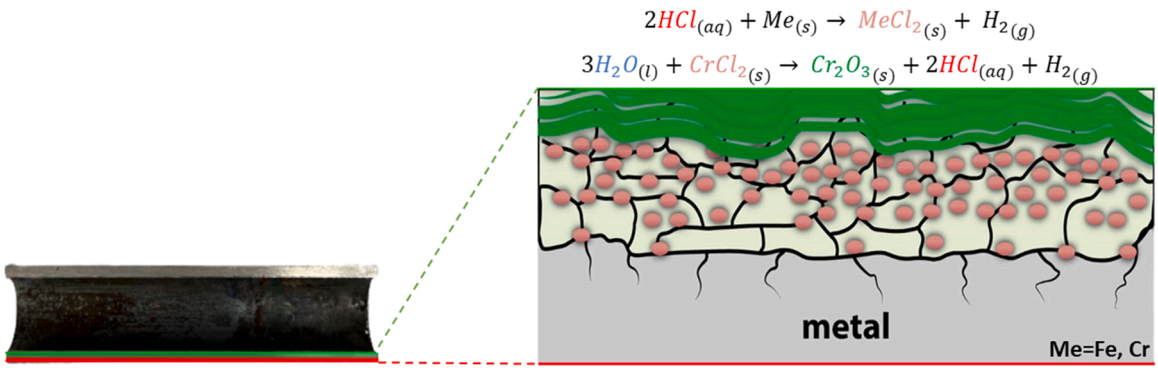

Fig. 9. Corrosion mechanism of SS-316 when exposed to HTDC process.
The mechanism is partially adapted from [44].

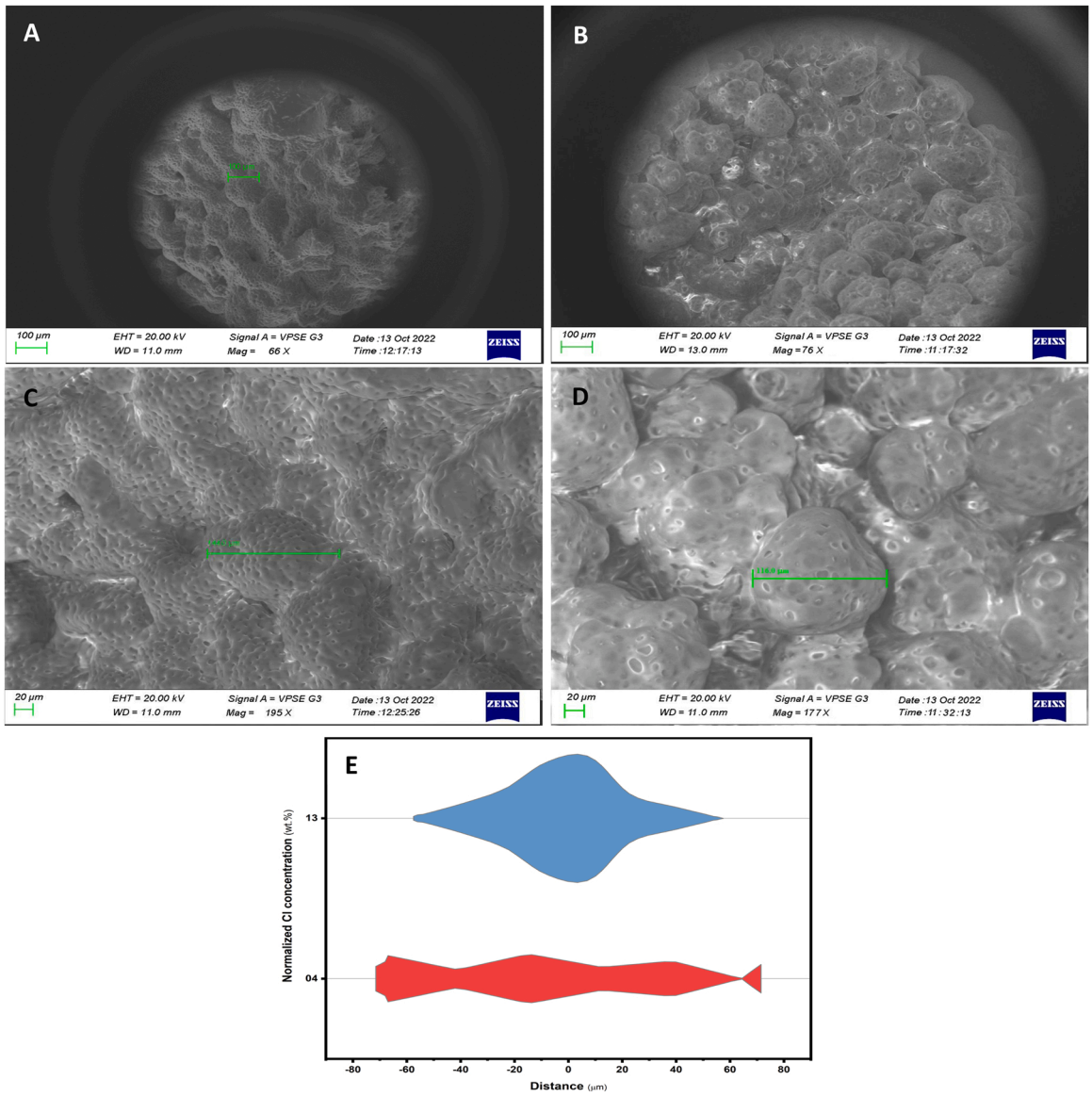

Fig. 10. SEM-EDX results; A and C) HTDC_NC_04, B and D) HTDC_NC_13, and E) Intraparticle distribution of Cl, based on mapping results.

dechlorination (Fig. 11A). This might introduce carbon rejection as the primary pathway for dechlorination, even though the literature lacks any concrete agreement regarding the impact of K_2CO_3 on the dechlorination of PVC [9,22,37,55].

The most intriguing discovery is attributed to the Ni catalysts, where the highest rate of Cl removal accompanies one of the lowest reactor wall corrosions with the lowest Cl/C and H/C molar ratios. Within the catalysis community, Ni-based catalysts are assumed to be highly active

Table 4
CCD optimization results: predicted vs. actual values.

	Optimum Operating condition			Experimental data		
	T (°C)	RT (min)	W/PVC (ratio)	Cl removal (%)	Fe in AP (g)	H/C molar ratio
Predicted	229.61	38.32	12.85	36.43	0.068	1.41
Actual	230	38	13	35.49 ± 1.06	0.072 ± 0.007	1.51 ± 0.14

in methanation reactions when they encounter waste materials (vide Table SM.8 in SMF) [56], a feature that HTDC can leverage for increased Cl removal via Carbon rejection. The high concentration of chloride ions, caused by severe dechlorination at high temperature and pressure, should have expectedly led to significant corrosion of Iron. However, the line chart in Fig. 11B shows a low corrosion rate for Ni-assisted dechlorination of PVC, which could have happened due to the interaction of Ni^{2+} ions with released Chlorides. Apart from Ni-catalyzed experiments, among the catalytic HTDC, the lowest dechlorination is associated with the lowest contribution of Fe in corrosion products (see Table SM.8 in SMF for a detailed concentration of each metal in aqueous products).

Moreover, reusing partially dechlorinated PVC, HTDC_NC_OPT, as the feedstock for the second round of chlorine removal yielded a promising result. The second stage HTDC, denoted as HTDC_NC_RC, has resulted in a lower H/C and Cl/C molar ratio, a higher O/C molar ratio, and a slightly reduced dechlorination compared to its counterparts performed under optimal operating conditions. Such recirculation led to a moderate Cl removal rate at a low expense of reactor corrosion.

Almost all the approaches used to promote Cl removal under optimal conditions, except Ni^{2+}-containing solutions, resulted in a significant corrosion rate, depending on the extent of dechlorination. Since ANOVA analysis revealed no significant correlation between PVC concentration and reactor wall corrosion in the non-catalytic optimization, one might assume that the number of chloride ions, rather than their concentration, is responsible for Fe leaching out of the reactor wall.

3.8.2. Thermal resistance and mass transfer

Fig. 12 depicts the thermal resistance of solid products from catalytic tests and virgin PVC in terms of TG and DTG curves, along with statistics derived from these curves acquired after the deconvolution of DTG branches. Furthermore, figures in the bar charts are ascribed to the area of deconvoluted peaks representing the remaining weight percent of the solid residues in question after exposing them to the temperature-programmed analysis.

There appears to be a significant difference in the DTG curves, with virgin PVC having three distinct peaks located in the temporal region of 290–650 °C and others having four peaks within nearly the same range. We attribute the first peak in the PVC pattern around 292 °C to the removal of Cl content because its area percentage closely matches the concentration of Cl in pure PVC. This weight fraction begins to shrink as the dechlorination proceeds, with the solid residue collected from the HTDC_Ni experiment contributing the least.

To our knowledge, PVC dechlorination during the hardly stable first thermal decomposition region may transform the polymer structure into a poly-aromatic polymer via radical and double bond formation[22]. Interestingly, our TG findings feature the formation of a recalcitrant new part in the solid residues detected in the virgin PVC powder. While PVC lacks such a hard-to-break part, samples collected from experiments done in the presence of Ni catalyst share the highest fraction among the catalytic experiments, followed by HTDC_NC_OPT and HTDC_NC_RC.

Images and charts in Fig. 13 depict the radial distribution of different elements in solid products obtained from catalytic tests to demonstrate whether there is a mass transfer limitation across PVC grains as they undergo HTDC in the presence of various catalysts.

In these diagrams, the Cl distribution still follows a mountain-like pattern across the grain intersection in both non-catalytic tests, HTDC_NC_OPT and HTDC_NC_RC. However, the catalytic dechlorination in the presence of Ni ions resulted in an almost flat distribution. Previous studies reasoned diffusion-controlled dechlorination of PVC for such curved patterns, as swelling significantly governs the process rate [22]. SEM images in Fig. 13 confirm the presence of such swelling in non-catalytic tests, even in the case of K_2CO_3 with low dechlorination efficiency, where the interfaces between two grains are distinguishable. However, when it comes to Ni, catalytic HTDC produced a porous network with no discernible interfaces.

3.9. Corrosion assessment according to Industrial standards

The following discussion aims to spot the position of catalytic HTDC of PVC in a related industry so that its material applicability can be easily identified. In search of an adequate indicator, we came across Equipment Service Lifetime, which represents the maximum number of days a chemical facility can safely operate [57]:

$$EstimatedServiceLifetime = \frac{Equipmentwallthickness(mils)}{Corrosionrate(mpy)} \quad (7)$$

This equation expresses the wall thickness and corrosion rate in mils (1 mil=0.001 in.) and mpy (mils per year). Because iron makes up the majority of the SS-316 alloy (see Table SM.9 in SMF), its corrosion rate was converted to mpy units to calculate the material lifetime (Fig. 14) [58].

There is no doubt in the scientific community that all concentrations of HCl can severely attack and destroy Stainless Steel alloys by vanishing the passive protective layer. However, in hot-compressed solutions, such as the HTDC medium, the alloys are rapidly attacked with hydrogen evolution, resulting in a severe corrosion rate of more than 2000 mpy at temperatures greater than 100 °C where even small amounts of hydrochloric acid exist in the aqueous environment[59]. Among the catalytic approaches used in this study, we observed that the higher the Iron Corrosion rate, the shorter the estimated lifetime. On the plus side, there are still K_2CO_3 and Recirculation experiments with the lowest Iron corrosion and, as a result, the highest expected operation time. However, several barriers remain for commercial application because the minimum Cl removal requirement of 96% must be combined with

Table 5
Elemental and TG analyses results.

RXN Metadata	Elemental Distribution							Cl removal (%)	Fe in AP (g)
	C (wt%)	H (wt%)	Cl (wt%)	O (wt%)	H/C	Cl/C	O/C		
HTDC_NC_OPT	41.24 ± 4.54	5.17 ± 1.29	39.47 ± 5.92	14.12 ± 2.40	1.51 ± 0.14	0.32 ± 0.08	0.26 ± 0.04	35.49 ± 1.06	0.072 ± 0.007
HTDC_NC_RC	45.69 ± 3.66	5.35 ± 1.07	29.62 ± 3.85	19.34 ± 4.45	1.41 ± 0.20	0.22 ± 0.04	0.32 ± 0.05	32.68 ± 1.31	0.004 ± 0.001
HTDC_TiO_2	36.92 ± 1.85	4.64 ± 0.84	41.74 ± 7.51	16.70 ± 2.00	1.51 ± 0.17	0.38 ± 0.09	0.34 ± 0.03	31.78 ± 1.11	0.065 ± 0.008
HTDC_K_2CO_3	39.34 ± 5.11	4.94 ± 1.04	47.29 ± 9.93	8.44 ± 1.60	1.51 ± 0.26	0.41 ± 0.06	0.16 ± 0.03	22.71 ± 0.34	0.003 ± 0.001
HTDC_Ni	58.11 ± 2.32	5.10 ± 0.97	13.01 ± 2.47	23.79 ± 5.95	1.05 ± 0.12	0.08 ± 0.01	0.31 ± 0.04	78.74 ± 3.12	0.033 ± 0.002
HTDC_Ni_60[a]	65.12 ± 6.51	4.65 ± 1.12	2.34 ± 0.33	23.89 ± 3.82	1.00 ± 0.11	0.01 ± 0.00	0.26 ± 0.03	96.18 ± 1.08	0.078 ± 0.004

[a] HTDC_NC_60 refers to HTDC of PVC in the presence of Ni catalyst that was done for an extended RT of 60 min

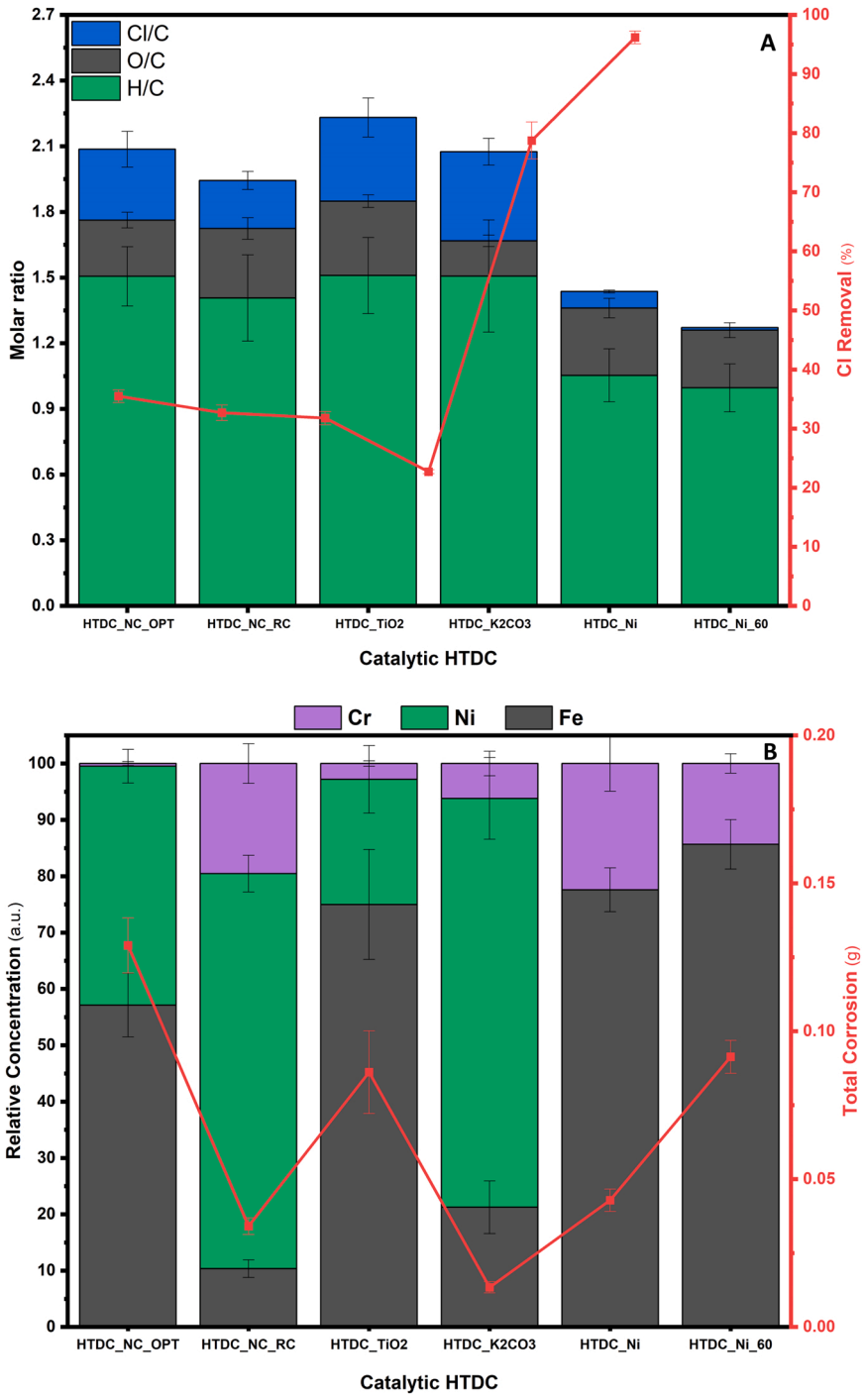

Fig. 11. HTDC results in the presence of catalysts; A) Molar ratio of elements in solid residues collected from catalytic HTDC of PVC along with Cl removal rate, B) Concentration of metals in AP.

significantly low reactor corrosion of 2–5 mpy [60].

4. Conclusion

The current work statistically proved the strongest influences of Temperature and Reaction Time on HTDC of PVC using RSM-assisted optimization, so their hidden interaction turned out to be significant as well. On the other hand, water content remained neutral in all operational aspects studied, including Cl removal rate, reactor wall corrosion, and H/C molar ratio. Undercover non-catalytic investigation, we proposed a mechanism for HTDC of PVC in which the severity of operating conditions was a game-changer. A high reaction severity tends to drive the Cl removal through an acid-catalyzed elimination route in which an aromatic network contributes more to the final dechlorinated product. From a material viewpoint, we discovered that in-situ produced aqueous solution of HCl tends to wear out Fe and Ni into the aqueous product while leaving a solid layer concentrated in Cr and Mo oxides on the inner surface of the reactor wall.

Although Ni-catalyzed HTDC removed more than 96% of the organic chlorine in PVC, it seemingly moved the Iron corrosion out of an industrially tolerable level by shortening the estimated service lifetime of the reactor to less than 80 days. This would be critical for those

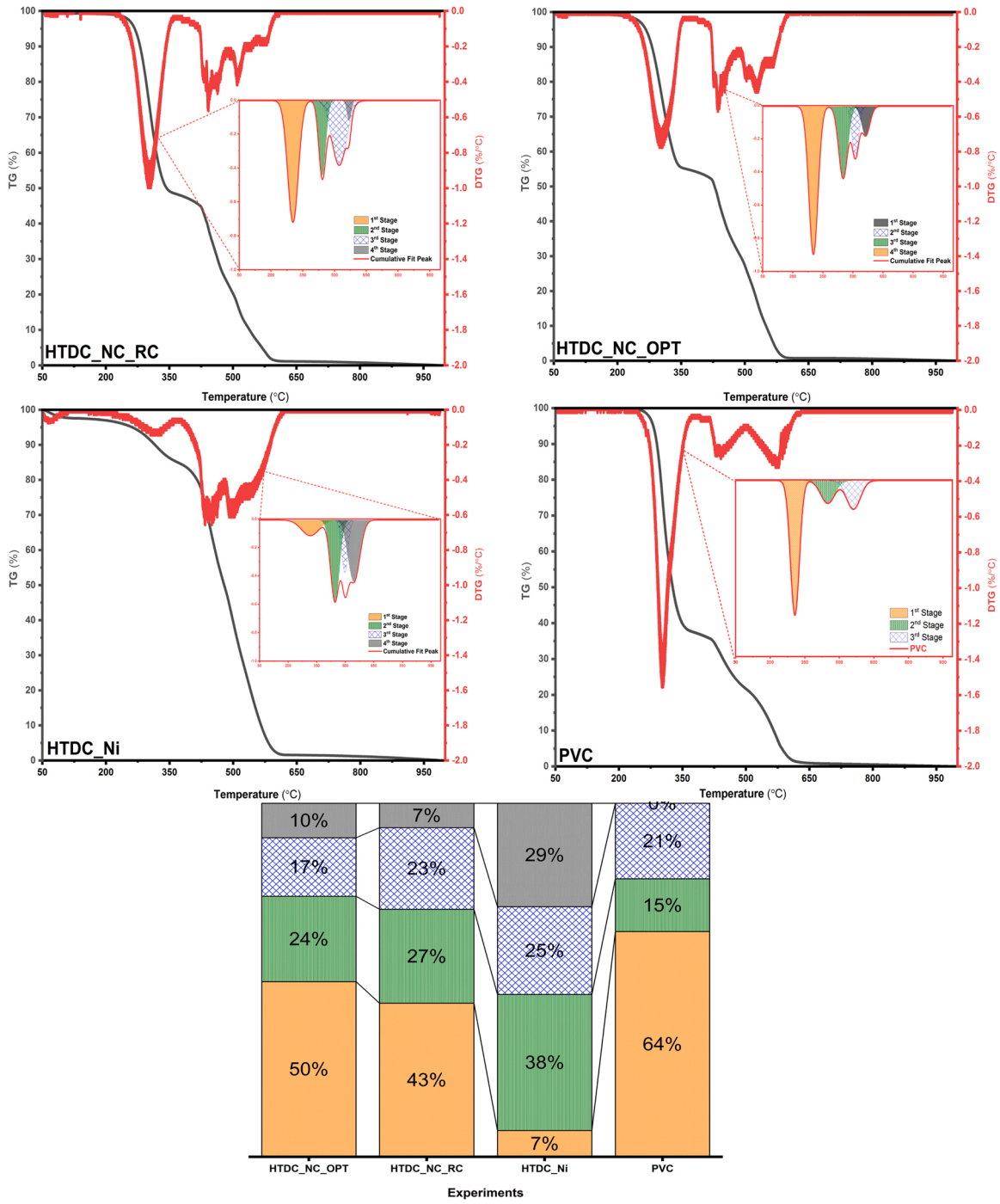

Fig. 12. TG results corresponded to selected catalytic products.

wanting to recover as much HCl as possible from PVC waste while making the solid waste a potential feedstock for fuel production or depolymerization plants and meeting the 1% requirement for RDFs in many developed countries. While chlorine detachment from the PVC backbone appears to be maturing from a chemistry standpoint if Ni^{2+} is present in sufficient quantities in the reaction medium, recirculation demonstrated promising results from a corrosion standpoint, with a moderate Cl removal of 35% accompanied by nearly 650 days of chemical equipment. More studies are yet to be performed to either mature the chemistry of the Recirculation approach to improve the Cl removal rate or to focus on the material perspectives of Ni-assisted dechlorination to diminish corrosion threat.

CRediT authorship contribution statement

Mohammad Salimi: Conceptualization, Investigation, Methodology, Supervision, Validation, Data curation, Visualization, Writing – original draft, Writing – review & editing. **Thomas Helmer Pedersen:** Validation. **Lasse Rosendahl:** Validation.

Declaration of Competing Interest

The authors declare that they have no known competing financial interests or personal relationships that could have appeared to influence the work reported in this paper.

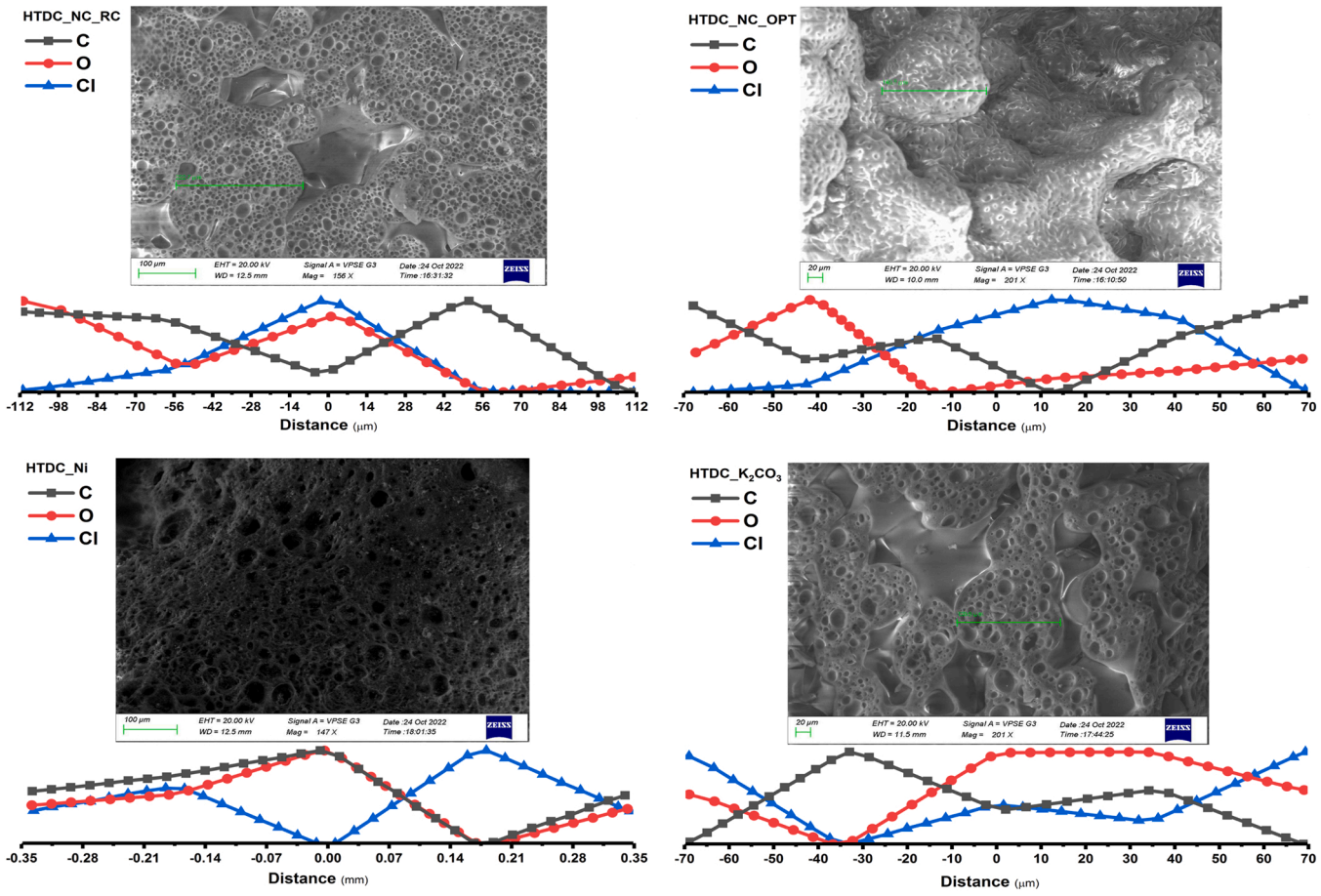

Fig. 13. SEM-EDX results in the case of selected catalytic products.

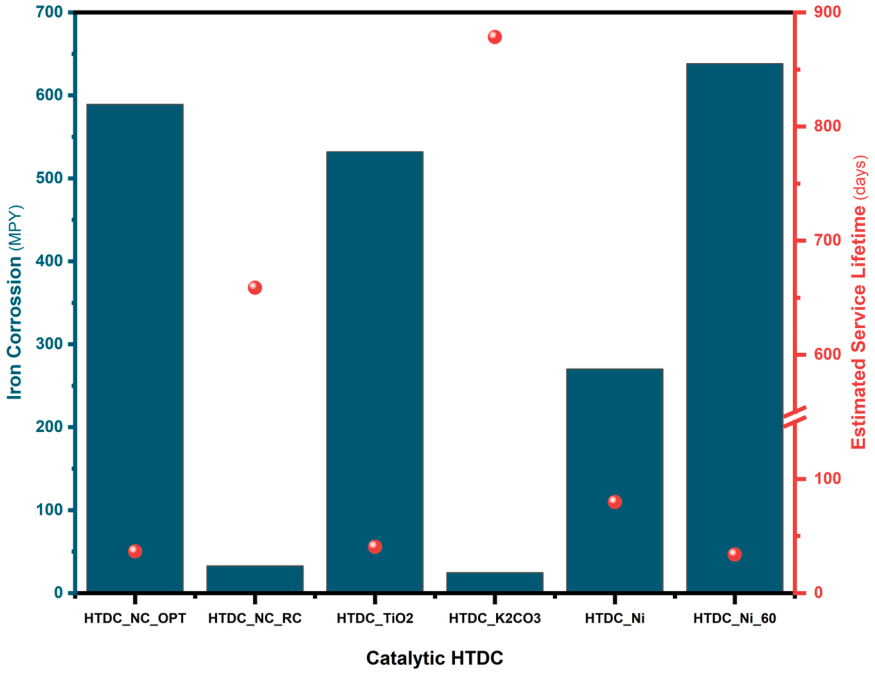

Fig. 14. Corrosiveness of catalytic HTDC experiments compared to industrial criteria.

Data availability

No data was used for the research described in the article.

Acknowledgment

CATALEPTIC project has recieved funding from the European Union's Horizon 2020 research and innovation programme under the Marie Skłodowska-Curie grant agreement No 101033386.
(https://cordis.europa.eu/project/id/101033386).

Appendix A. Supporting information

Supplementary data associated with this article can be found in the online version at doi:10.1016/j.jece.2023.109783.

References

[1] J.P. da Costa, P.S.M. Santos, A.C. Duarte, T. Rocha-Santos, (Nano)plastics in the environment – Sources, fates and effects, Sci. Total Environ. 566– 567 (2016) 15–26, https://doi.org/10.1016/J.SCITOTENV.2016.05.041.
[2] Y. Miao, A. von Jouanne, A. Yokochi, Current Technologies in Depolymerization Process and the Road Ahead, Polymers 2021, Vol. 13, Page 449. 13 (2021) 449. https://doi.org/10.3390/POLYM13030449.
[3] S.D. Anuar Sharuddin, F. Abnisa, W.M.A. Wan Daud, M.K. Aroua, A review on pyrolysis of plastic wastes, Energy Convers. Manag 115 (2016) 308–326, https://doi.org/10.1016/J.ENCONMAN.2016.02.037.
[4] F.R. Xiu, Y. Wang, X. Yu, Y. Li, Y. Lu, K. Zhou, J. He, Z. Song, X. Gao, A novel safety treatment strategy of DEHP-rich flexible polyvinyl chloride waste through low-temperature critical aqueous ammonia treatment, Sci. Total Environ. 708 (2020), 134532, https://doi.org/10.1016/J.SCITOTENV.2019.134532.
[5] J. Miliute-Plepiene, A. Fråne, A.M. Almasi, Overview of polyvinyl chloride (PVC) waste management practices in the Nordic countries, Clean. Eng. Technol. 4 (2021), 100246, https://doi.org/10.1016/J.CLET.2021.100246.
[6] R. Chand, K. Kohansal, S. Toor, T.H. Pedersen, J. Vollertsen, Microplastics degradation through hydrothermal liquefaction of wastewater treatment sludge, J. Clean. Prod. 335 (2022), 130383, https://doi.org/10.1016/J.JCLEPRO.2022.130383.
[7] P. Zhao, Z. Li, T. Li, W. Yan, S. Ge, The study of nickel effect on the hydrothermal dechlorination of PVC, J. Clean. Prod. 152 (2017) 38–46, https://doi.org/10.1016/J.JCLEPRO.2017.03.101.
[8] B. Cao, Y. Sun, J. Guo, S. Wang, J. Yuan, S. Esakkimuthu, B. Bernard Uzoejinwa, C. Yuan, A.E.F. Abomohra, L. Qian, L. Liu, B. Li, Z. He, Q. Wang, Synergistic effects of co-pyrolysis of macroalgae and polyvinyl chloride on bio-oil/bio-char properties and transferring regularity of chlorine, Fuel 246 (2019) 319–329, https://doi.org/10.1016/J.FUEL.2019.02.037.
[9] G. Gandon-Ros, A. Soler, I. Aracil, M.F. Gómez-Rico, Dechlorination of polyvinyl chloride electric wires by hydrothermal treatment using K2CO3 in subcritical water, Waste Manag. 102 (2020) 204–211, https://doi.org/10.1016/J.WASMAN.2019.10.050.
[10] E.M. Zakharyan, N.N. Petrukhina, A.L. Maksimov, Pathways of chemical recycling of polyvinyl chloride: part 1, Russ. J. Appl. Chem. 93 (2020) 1271–1313, https://doi.org/10.1134/S1070427220090013/TABLES/8.
[11] J.S. dos Passos, M. Glasius, P. Biller, Screening of common synthetic polymers for depolymerization by subcritical hydrothermal liquefaction, Process Saf. Environ. Prot. 139 (2020) 371–379, https://doi.org/10.1016/J.PSEP.2020.04.040.
[12] F.R. Xiu, Y. Lu, Y. Qi, DEHP degradation and dechlorination of polyvinyl chloride waste in subcritical water with alkali and ethanol: A comparative study, Chemosphere 249 (2020), 126138, https://doi.org/10.1016/J.CHEMOSPHERE.2020.126138.
[13] Z. Yao, X. Ma, A new approach to transforming PVC waste into energy via combined hydrothermal carbonization and fast pyrolysis, Energy 141 (2017) 1156–1165, https://doi.org/10.1016/J.ENERGY.2017.10.008.
[14] A. Soler, J.A. Conesa, N. Ortuño, Application of Subcritical Water to Dechlorinate Polyvinyl Chloride Electric Wires, Energies 2018, Vol. 11, Page 2612. 11 (2018) 2612. https://doi.org/10.3390/EN11102612.
[15] D. Ma, L. Liang, E. Hu, H. Chen, D. Wang, C. He, Q. Feng, Dechlorination of polyvinyl chloride by hydrothermal treatment with cupric ion, Process Saf. Environ. Prot. 146 (2021) 108–117, https://doi.org/10.1016/J.PSEP.2020.08.040.
[16] P. Zhao, T. Li, W. Yan, L. Yuan, Dechlorination of PVC wastes by hydrothermal treatment using alkaline additives, Https://Doi.Org/10.1080/09593330.2017.1317841. 39 (2017) 977–985. https://doi.org/10.1080/09593330.2017.1317841.
[17] H. Peng, Z. Luo, L. Li, al -, C. Chenggong, Z. Weixin, W. Jing, W. Zhang, H. Chen, Q. Peng, R. Fan, W. Zhang, Y. Wang, D. Chen, Y.Zhang, Metal Material Resistant to Hydrochloric Acid Corrosion, J Phys Conf Ser. 1732 (2021) 012134. https://doi.org/10.1088/1742–6596/1732/1/012134.
[18] Y. Wang, F. Gao, J. Yang, Y. Zhu, C. Fang, S. Wang, G. Zhao, Comparative study on corrosion characteristics of Al2O3/316L and TiO2/316L stainless steel in supercritical water, Int J. Hydrog. Energy 42 (2017) 19836–19842, https://doi.org/10.1016/J.IJHYDENE.2017.06.129.
[19] M. Šípová, D. Marušáková, C. Aparicio, J. Procházka, P. Halodová, A study on the corrosion behaviour of stainless steel 08Cr18Ni10Ti in supercritical water, Corros. Sci. 211 (2023), 110853, https://doi.org/10.1016/J.CORSCI.2022.110853.
[20] M.M. Wang, C.C. Zhang, F.S. Zhang, Recycling of spent lithium-ion battery with polyvinyl chloride by mechanochemical process, Waste Manag. 67 (2017) 232–239, https://doi.org/10.1016/J.WASMAN.2017.05.013.
[21] F.R. Xiu, X. Tan, Y. Qi, M. Wang, Treatment of DEHP-rich PVC waste in subcritical urine wastewater: Efficient dechlorination, denitrification, plasticizer decomposition, and preparation of high-purity phthalic acid crystals, J. Hazard Mater. 441 (2023), 129820, https://doi.org/10.1016/J.JHAZMAT.2022.129820.
[22] E.M. Zakharyan, N.N. Petrukhina, E.G. Dzhabarov, A.L. Maksimov, Pathways of Chemical Recycling of Polyvinyl Chloride. Part 2, Russ. J. Appl. Chem. 93 (2020) 1445–1490, https://doi.org/10.1134/S1070427220100018/SCHEMES/2.
[23] M.B.I. Chowdhury, Nickel-based Catalysts for Gasification of Glucose in Supercritical Water., (2010).
[24] R.R. Shetty, S.S. Raut, P.S. Kulkarni, S.P. Kamble, Hydrodechlorination of 4-Chloro-2-aminophenol into a recyclable product using Ni- and Cu-based catalysts, Ind. Eng. Chem. Res 61 (2022) 14433–14445, https://doi.org/10.1021/ACS.IECR.2C00848/ASSET/IMAGES/LARGE/IE2C00848_0016.JPEG.
[25] S.S. Raut, R. Shetty, N.M. Raju, S.P. Kamble, P.S. Kulkarni, Screening of zero valent mono/bimetallic catalysts and recommendation of Raney Ni (without reducing agent) for dechlorination of 4-chlorophenol, Chemosphere 250 (2020), 126298, https://doi.org/10.1016/J.CHEMOSPHERE.2020.126298.
[26] D.C. Montgomery, Design and Analysis of Experiments, 10th Edition, Wiley, Wiley. (2020) 1–682. https://www.wiley.com/en-us/Design+and+Analysis+of+Experiments%2C+10th+Edition-p-9781119492443 (accessed October 30, 2022).
[27] P. Zhao, Z. Li, T. Li, W. Yan, S. Ge, The study of nickel effect on the hydrothermal dechlorination of PVC, J. Clean. Prod. 152 (2017) 38–46, https://doi.org/10.1016/J.JCLEPRO.2017.03.101.
[28] X. Ma, Y. Liu, X. Li, J. Xu, G. Gu, C. Xia, Water: the most effective solvent for liquid-phase hydrodechlorination of chlorophenols over Raney Ni catalyst, Appl. Catal. B 165 (2015) 351–359, https://doi.org/10.1016/J.APCATB.2014.10.035.
[29] J. Poerschmann, B. Weiner, S. Woszidlo, R. Koehler, F.D. Kopinke, Hydrothermal carbonization of poly(vinyl chloride, Chemosphere 119 (2015) 682–689, https://doi.org/10.1016/J.CHEMOSPHERE.2014.07.058.
[30] M. Salimi, A. Tavasoli, L. Rosendahl, Optimization of γ-alumina porosity via response surface methodology: the influence of engineering support on the performance of a residual oil hydrotreating catalyst, Microporous Mesoporous Mater. (2020), 110124, https://doi.org/10.1016/j.micromeso.2020.110124.
[31] M. Salimi, S. Balou, K. Kohansal, K. Babaei, A. Tavasoli, M. Andache, Optimizing the preparation of Meso- and microporous canola stalk-derived hydrothermal carbon via response surface methodology for methylene blue removal, Energy Fuels 31 (2017) 12327–12338, https://doi.org/10.1021/acs.energyfuels.7b02440.
[32] M.A. Kassim, T.K. Meng, R. Kamaludin, A.H. Hussain, N.A. Bukhari, Bioprocessing of sustainable renewable biomass for bioethanol production, Value-Chain of Biofuels: Fundamentals, Technology, and Standardization. (2022) 195–234. https://doi.org/10.1016/B978–0-12–824388-6.00004-X.
[33] ASTM International, ASTM D5291 - 16 Standard Test Methods for Instrumental Determination of Carbon, Hydrogen, and Nitrogen in Petroleum Products and Lubricants, (2016). https://doi.org/https://10.1520/D5291–16.
[34] User, Chloride.docx SI Analytics-Application report Titration Titration of Chloride Description, (n.d.).
[35] Analytical Methods for Atomic Absorption Spectroscopy, (1996).
[36] J. Lu, S. Borjigin, S. Kumagai, T. Kameda, Y. Saito, T. Yoshioka, Practical dechlorination of polyvinyl chloride wastes in NaOH/ethylene glycol using an up-scale ball mill reactor and validation by discrete element method simulations, Waste Manag. 99 (2019) 31–41, https://doi.org/10.1016/J.WASMAN.2019.08.034.
[37] J.D. Fonseca, G. Grause, T. Kameda, T. Yoshioka, Effects of steam on the thermal dehydrochlorination of poly(vinyl chloride) resin and flexible poly(vinyl chloride) under atmospheric pressure, Polym. Degrad. Stab. 117 (2015) 8–15, https://doi.org/10.1016/J.POLYMDEGRADSTAB.2015.03.011.
[38] J. Poerschmann, B. Weiner, S. Woszidlo, R. Koehler, F.D. Kopinke, Hydrothermal carbonization of poly(vinyl chloride, Chemosphere 119 (2015) 682–689, https://doi.org/10.1016/J.CHEMOSPHERE.2014.07.058.
[39] J. Zhou, B. Gui, Y. Qiao, J. Zhang, W. Wang, H. Yao, Y. Yu, M. Xu, Understanding the pyrolysis mechanism of polyvinylchloride (PVC) by characterizing the chars produced in a wire-mesh reactor, Fuel 166 (2016) 526–532, https://doi.org/10.1016/J.FUEL.2015.11.034.
[40] D. Ma, L. Liang, E. Hu, H. Chen, D. Wang, C. He, Q. Feng, Dechlorination of polyvinyl chloride by hydrothermal treatment with cupric ion, Process Saf. Environ. Prot. 146 (2021) 108–117, https://doi.org/10.1016/J.PSEP.2020.08.040.
[41] S. Kang, X. Li, J. Fan, J. Chang, Characterization of hydrochars produced by hydrothermal carbonization of lignin, cellulose, d-Xylose, and wood meal, Ind. Eng. Chem. Res 51 (2012) 9023–9031, https://doi.org/10.1021/IE300565D.
[42] Z.A. Mayer, A. Apfelbacher, A. Hornung, Effect of sample preparation on the thermal degradation of metal-added biomass, J. Anal. Appl. Pyrolysis 94 (2012) 170–176, https://doi.org/10.1016/J.JAAP.2011.12.008.
[43] D. Ma, L. Liang, E. Hu, H. Chen, D. Wang, C. He, Q. Feng, Dechlorination of polyvinyl chloride by hydrothermal treatment with cupric ion, Process Saf. Environ. Prot. 146 (2021) 108–117, https://doi.org/10.1016/J.PSEP.2020.08.040.
[44] A. Schmid, G. Mori, E. Bucher, R. Haubner, Model about the course of corrosion reactions of austenitic steels in H 2 S-, HCl- and CO 2 -containing atmospheres at 680 °C, Oxid. Met. 91 (2019) 1–10, https://doi.org/10.1007/S11085-018-9876-Z/FIGURES/5.

[45] M. Hjiri, Highly sensitive NO2 gas sensor based on hematite nanoparticles synthesized by sol–gel technique, J. Mater. Sci.: Mater. Electron. 31 (2020) 5025–5031, https://doi.org/10.1007/S10854-020-03069-4/TABLES/1.
[46] Z. Cao, C. Zuo, Cr2O3/carbon nanosheet composite with enhanced performance for lithium ion batteries, RSC Adv. 7 (2017) 40243–40248, https://doi.org/10.1039/C7RA06188A.
[47] J. Wang, G. Meng, K. Tao, M. Feng, X. Zhao, Z. Li, H. Xu, D. Xia, J.R. Lu, Immobilization of lipases on alkyl silane modified magnetic nanoparticles: effect of alkyl chain length on enzyme activity, PLoS One 7 (2012), e43478, https://doi.org/10.1371/JOURNAL.PONE.0043478.
[48] F. Taghizadeh, F. Taghizadeh, The study of structural and magnetic properties of NiO nanoparticles, Opt. Photonics J. 6 (2016) 164–169, https://doi.org/10.4236/OPJ.2016.68B027.
[49] Y. Hirano, Y. Kasai, K. Sagata, Y. Kita, Unique Approach for Transforming Glucose to C3 Platform Chemicals Using Metallic Iron and a Pd/C Catalyst in Water, Http://Dx.Doi.Org/10.1246/Bcsj.20160114. 89 (2016) 1026–1033. https://doi.org/10.1246/BCSJ.20160114.
[50] T. Li, P. Zhao, M. Lei, Z. Li, Understanding Hydrothermal Dechlorination of PVC by Focusing on the Operating Conditions and Hydrochar Characteristics, Applied Sciences 2017, Vol. 7, Page 256. 7 (2017) 256. https://doi.org/10.3390/APP7030256.
[51] T. Yoshioka, T. Kameda, G. Grause, S. Imai, A. Okuwaki, Effect of compatibility between solvent and poly(vinyl chloride) on dechlorination of poly(vinyl chloride), J. Polym. Res. 17 (2010) 489–493, https://doi.org/10.1007/S10965-009-9335-2/FIGURES/3.
[52] McKinsey & Company, The new plastics economy: A Danish research, innovation and business opportunity | McKinsey, 2019. ⟨https://www.mckinsey.com/featured-insights/europe/the-new-plastics-economy-a-danish-research-innovation-and-business-opportunity⟩ (accessed November 1, 2022).
[53] F.R. Xiu, X. Yu, Y. Qi, A high-efficiency and low-temperature subcritical water dechlorination strategy of polyvinyl chloride using coal fly ash (CFA) and coal gangue (CG) as enhancers, J. Clean. Prod. 260 (2020), 121085, https://doi.org/10.1016/J.JCLEPRO.2020.121085.
[54] V.D. Fikhman, E.Y. Vaiman, A.B. Pakshver, K.S. Minsker, Dehydrochlorination kinetics of polyvinylchloride (PVC) solutions in dimethylformamide, Polym. Sci. U. S. S. R. 14 (1972) 2769–2779, https://doi.org/10.1016/0032-3950(72)90206-7.
[55] J. Lu, S. Borjigin, S. Kumagai, T. Kameda, Y. Saito, T. Yoshioka, Practical dechlorination of polyvinyl chloride wastes in NaOH/ethylene glycol using an up-scale ball mill reactor and validation by discrete element method simulations, Waste Manag. 99 (2019) 31–41, https://doi.org/10.1016/J.WASMAN.2019.08.034.
[56] M. Salimi, A. Tavasoli, S. Balou, H. Hashemi, K. Kohansal, Influence of promoted bimetallic Ni-based catalysts and Micro/Mesopores carbonaceous supports for biomass hydrothermal conversion to H2-rich gas, Appl. Catal. B 239 (2018) 383–397, https://doi.org/10.1016/j.apcatb.2018.08.039.
[57] W.S. Tait, Controlling Corrosion of Chemical Processing Equipment, Handbook of Environmental Degradation Of Materials: Third Edition. (2018) 583–600. https://doi.org/10.1016/B978–0-323–52472-8.00028–9.
[58] Corrosion rate conversion, (n.d.). https://corrosion-doctors.org/Principles/Conversion.htm (accessed November 26, 2022).
[59] CORROSION RESISTANCE O.F. THE AUSTENITIC CHROMIUM-NICKEL STAINLESS STEELS IN CHEMICAL ENVIRONMENTS, (n.d.).
[60] Corrosion Monitoring WHY SHOULD I USE A CORROSION RACK?, (n.d.).